Benzisothiazolinone Derivatives as Potent Allosteric Monoacylglycerol Lipase Inhibitors That Functionally Mimic Sulfenylation of Regulatory Cysteines

Benzisothiazolinone derivatives as potent allosteric monoacylglycerol lipase inhibitors that functionally mimic sulfenylation of regulatory cysteines

Riccardo Castelli,[1] Laura Scalvini,[1] Federica Vacondio,[1,2] Alessio Lodola,[1] Mattia Anselmi,[1] Stefano Vezzosi,[1] Caterina Carmi,[1] Michele Bassi,[1] Francesca Ferlenghi,[1,2] Silvia Rivara,[1,2,*] Ingvar R. Møller,[3] Kasper D. Rand,[3] Jennifer Daglian,[4] Don Wei,[4] Emmanuel Y. Dotsey,[4] Faizy Ahmed,[4] Kwang-Mook Jung,[4] Nephi Stella,[5] Simar Singh,[5] Marco Mor,[1,2] Daniele Piomelli[4,6,7,8]

[1] Dipartimento di Scienze degli Alimenti e del Farmaco, Università degli Studi di Parma, Parco Area delle Scienze 27/A, I-43124 Parma, Italy

[2] Centro Interdipartimentale Biopharmanet-tec, Università degli Studi di Parma, Parco Area delle Scienze, Tecnopolo Padiglione 33, I-43124 Parma, Italy

[3] Department of Pharmacy, Universitetsparken 2, DK-2100 Copenhagen

[4] Department of Anatomy and Neurobiology, School of Medicine, University of California, Irvine, California 92697, United States

[5] Department of Pharmacology, Psychiatry and Behavioral Sciences, University of Washington, Seattle, WA 98195-7280, United States.

[6] Departments of Biological Chemistry and Pharmacology, School of Medicine, University of California, Irvine, California 92697, United States

[7] Center for the Study of Cannabis, University of California, Irvine, California 92697, United States

[8] Visiting Professor, Università degli Studi di Parma under the TeachInParma project.

Abstract

We describe a set of benzisothiazolinone (BTZ) derivatives that are potent inhibitors of monoacylglycerol lipase (MGL), the primary degrading enzyme for the endocannabinoid 2-arachidonoyl-*sn*-glycerol (2-AG). Structure-activity relationship studies evaluated various substitutions on the nitrogen atom and the benzene ring of the BTZ nucleus. Optimized derivatives with nanomolar potency allowed to investigate the mechanism of MGL inhibition. Site-directed mutagenesis and mass spectrometry experiments showed that BTZs interact in a covalent reversible manner with regulatory cysteines, Cys201 and Cys208, causing a reversible sulfenylation known to modulate MGL activity. Metadynamics simulations revealed that BTZ adducts favor a closed conformation of MGL that occludes substrate recruitment. The BTZ derivative **13** protected neuronal cells from oxidative stimuli and increased 2-AG levels in mouse brain. The results identify Cys201 and Cys208 as key regulators of MGL function, and point to the BTZ scaffold as a useful starting point for the discovery of allosteric MGL inhibitors.

Introduction

Monoacylglycerol lipase (MGL) is a serine hydrolase that cleaves medium- and long-chain monoacylglycerols into fatty acid and glycerol, with the highest rate for arachidonic acid derivatives.[1] MGL expression is widespread in the body, and particularly high in the central nervous system (CNS) where it is exclusively localized to presynaptic nerve terminals.[2] In peripheral tissues, MGL serves two main functions: it mediates the last step in hormone-dependent lipolysis and contributes to the release of energy-rich fatty acids from triacylglycerol stores[3] and, secondly, it controls platelet aggregation by regulating the availability of non-esterified arachidonate for thromboxane A_2 biosynthesis.[4] By contrast, the primary role of MGL in the CNS is

to catalyze the hydrolytic deactivation of 2-arachidonoyl-*sn*-glycerol (2-AG),[5,6,7] an endogenous agonist at CB_1 and CB_2 cannabinoid receptors and the most abundant endocannabinoid found in the mammalian brain.[8,9] 2-AG is released upon demand from postsynaptic neurons and acts as a retrograde messenger to modulate presynaptic activity by engaging CB_1 cannabinoid receptors on axon terminals.[10] This signaling modality is thought to underpin most of the effects elicited by 2-AG in neural tissue, including antinociception,[11,12] neuroprotection,[13,14] and reduced anxiety.[15] In addition to these central CB_1-mediated actions, 2-AG also acts on peripheral CB_1 and CB_2 receptors to mediate, among other effects, immune modulation[16,17] and inhibition of cancer cell growth.[18,19]

The first MGL inhibitor to be reported was the carbamate derivative URB602 **1** (Figure 1), which acts through a partially reversible, noncompetitive mechanism.[20,21,22] More potent and selective compounds were subsequently discovered, which differ mechanistically from URB602 in that they inhibit MGL activity by forming covalent adducts with the enzyme's catalytic serine (Ser122). These molecules include carbamate derivatives such as JZL184 (**2**),[23] PF-06795071 (**3**)[24] and ABX-1431.[25] Recently, reversible MGL inhibitors have also been described, such as benzoylpiperidine derivatives[26] and piperazinyl pyrrolidin-2-ones.[27]

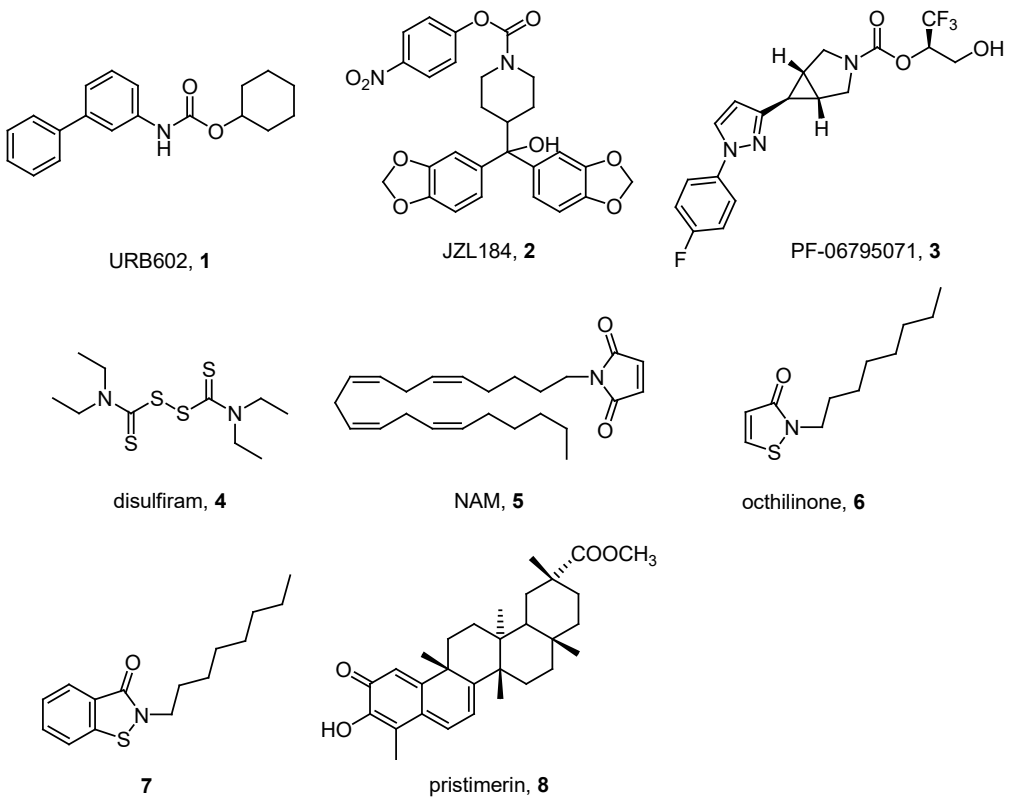

Figure 1. Chemical structures of current MGL inhibitors.

MGL is a member of the α/β hydrolases superfamily of enzymes[28] and requires a Ser/His/Asp triad for its catalytic activity.[29,30] An interesting structural feature of this enzyme is the presence of a lid domain that surrounds and hides its catalytic core. Within this domain, a region comprising helix α4 and the loop connecting helices α4 and α5 forms a flexible, hydrophobic U-shaped domain, which may serve both as a portal restricting or allowing the access of substrate into the catalytic site, and as a lipid-binding surface that reversibly interacts with membranes, where the substrate resides (Figure 2). Another characteristic of MGL is the presence of three cysteine residues – Cys242, Cys201 and Cys208 – that modulate catalytic activity in important ways. Cys242 is located close to the catalytic Ser122 and is directly involved in catalysis, as both its mutation and its covalent modification strongly reduce MGL's hydrolytic activity.[31] Indeed, computational and mass spectrometry studies have shown that the cysteine-reactive agent *N*-arachidonylmaleimide (NAM, **5**, Figure 1) forms a covalent adduct with this cysteine residue. [32,33,34] It is likely that other Michael

acceptors and disulfide-containing compounds, such as tetraethyluram disulphide (disulfiram, **4**, Figure 1), which inhibit MGL activity, act through a similar mechanism.[35] Unlike Cys242, Cys201 and Cys208 lie at a distance from the active site. Cys201 is located on the loop connecting helices α5 and α6, while Cys208 is on the first turn of helix α6, close to the putative position of the membrane bilayer (Figure 2). These cysteine residues are known allosteric modulators of rat and human MGL activity.[36] When rat MGL is exposed to relatively low concentrations of the intracellular messenger hydrogen peroxide,[37,38] Cys201 and Cys208 undergo reversible sulphenylation and the enzyme experiences a parallel decrease in catalytic activity.[39] This modulatory effect may be of physiological significance and it has been linked to the ability of covalent modifications of Cys201 and Cys208 to affect the interfacial activation of MGL by promoting the closure of the lid domain and reducing substrate recruitment.[40] The relevance of these regulatory cysteines has been further highlighted by the discovery that several reversible MGL inhibitors require Cys201 and Cys208 for activity. These include octyl-isothiazolinone (octhilinone, **6**) and octyl-benzisothiazolinone (**7**),[41,42] as well as the sesquiterpene pristimerin (**8**).[36]

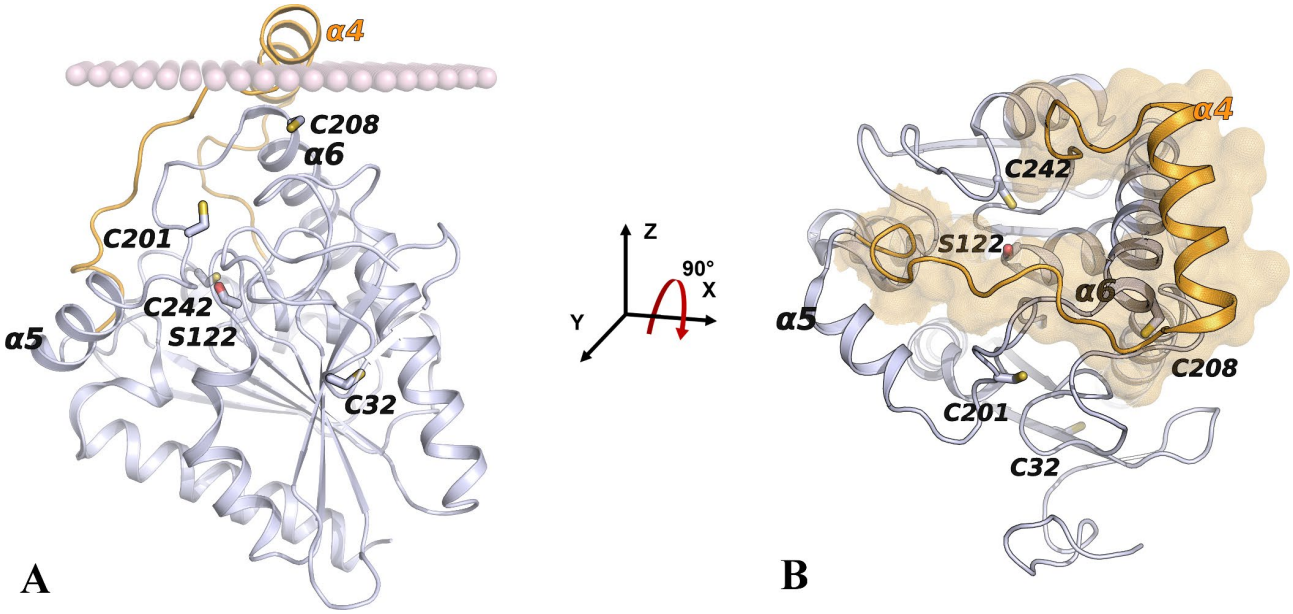

Figure 2. (**A**) The crystal structure of human MGL with the lid domain in its open conformation (PDB 3HJU) is shown in grey with the U-shaped access funnel to the catalytic site in orange. The

membrane profile is represented with light-pink spheres. (**B**) Helix α4 and the loop connecting helices α4 and α5 delineate a wide U-shaped structure that delimits the substrate access to the catalytic site.

The findings outlined above suggest that molecular probes that interact with regulatory cysteines Cys201 and Cys208 may offer important insights on the functioning of MGL as well as an alternative strategy to inhibit its activity. To test this idea, in the present study we introduced selected modifications in the structure of the BTZ derivative **7** with three interrelated objectives: i) enhance recognition by MGL and improve inhibitory potency; ii) define the molecular mechanism through which BTZs interact with MGL; iii) identify new probes that may guide the discovery of reversible allosteric MGL-targeting agents with potential therapeutic utility.

Chemistry

The synthesis of BTZs was performed as outlined in Schemes 1-3. Compounds **10**,[43] and **10a** were obtained *via* alkylating commercially available **9** with potassium carbonate and the appropriate iodoalkane. Compound **11** was obtained from **10a** by reacting the 6-chlorohexyl moiety with piperidine (Scheme 1). Compounds **13-16** were synthesized from freshly prepared 2-chlorosulfenylbenzoyl chloride **12**,[44] with the respective amine. 2-Phenylethyl isothiazolinone **18** was prepared according to a previously reported procedure.[45]

Scheme 1[a]

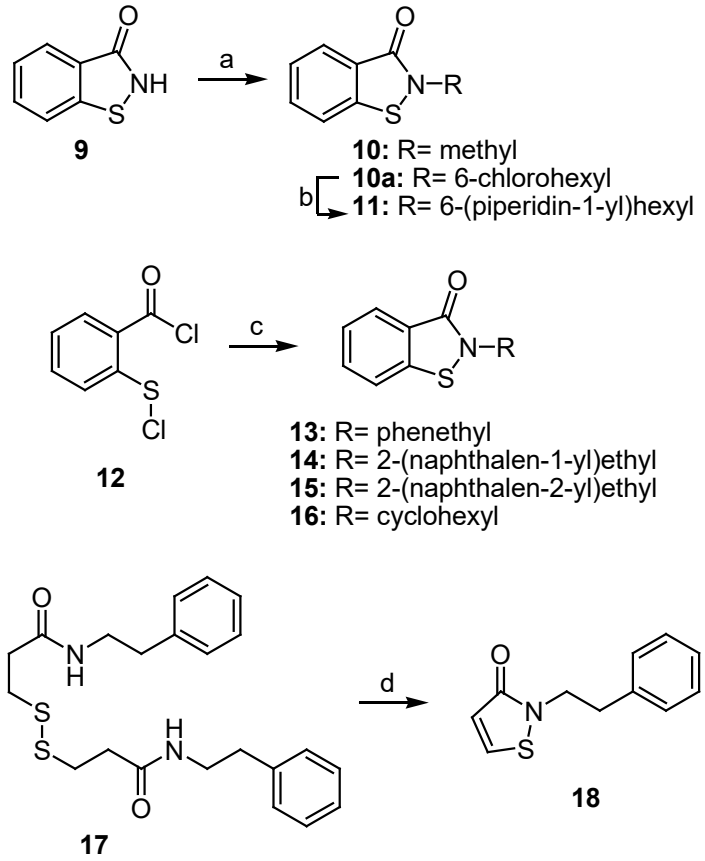

[a]Reagents and conditions: a) K_2CO_3, alkyl halide, MeCN, rt, 16 h; b) piperidine, K_2CO_3, KI, MeCN, 60 °C, 16 h; c) amine, anhydrous TEA, DCM rt, 16 h; d) SO_2Cl_2, anhydrous DCE 0 °C, 2 h.

Phenyl-substituted BTZs **24-30** were synthesized with a unified approach as outlined in Scheme 2.

Scheme 2[a]

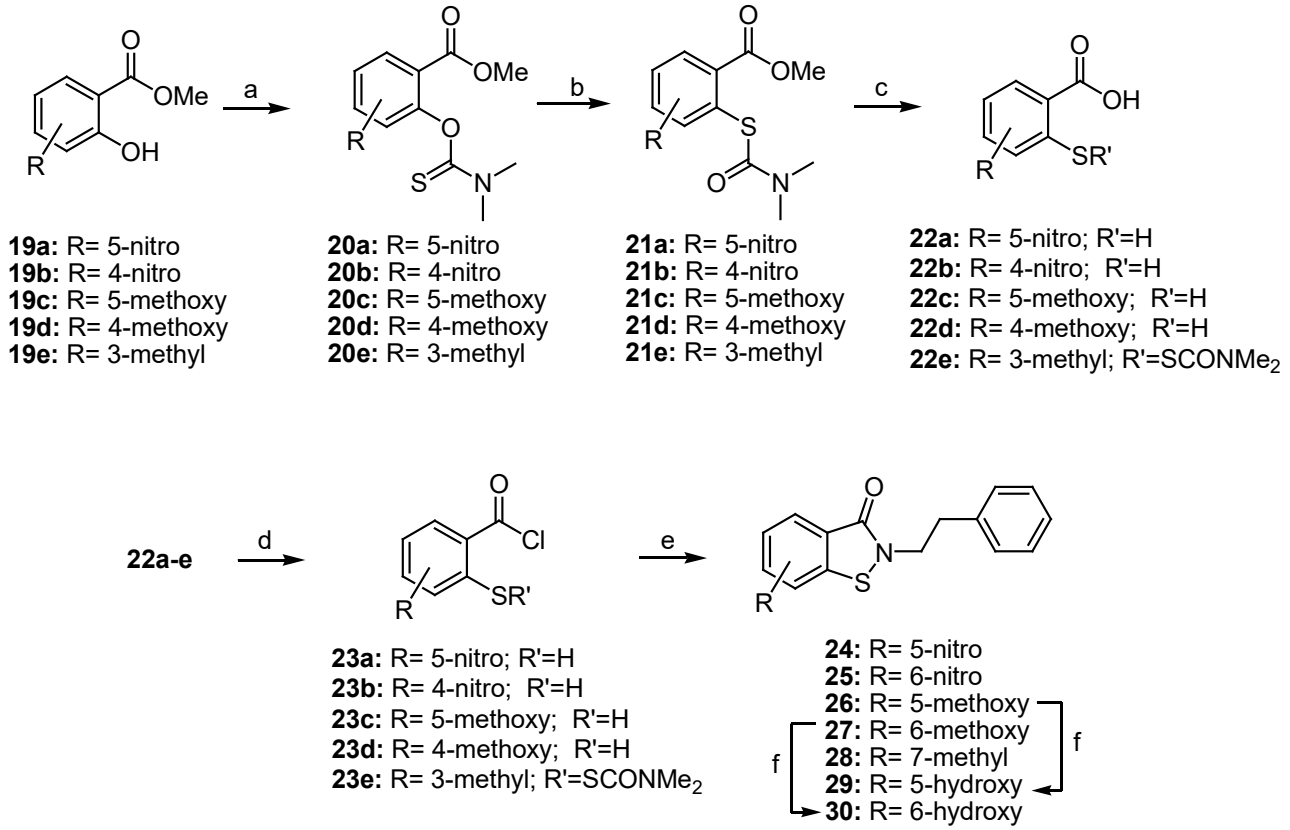

[a]Reagents and conditions: a) base, *N*,*N*-dithiocarbamoylchloride, anhydrous DMF; b) diphenylether; μW irradiation c) NaOH, MeOH/H_2O 2:1 v/v, reflux; d) $SOCl_2$, reflux, 6 h; e) *i*) 2-phenylethylamine, anhydrous TEA, THF *ii*) I_2, anhydrous THF, 0 °C to rt, 20 h; f) BBr_3, anhydrous benzene, 0 °C to reflux, 3 h.

Commercially available methyl salicylates **19a-e** were reacted with *N,N*-dithiocarbamoyl chloride in the presence of a base, either DABCO (**19a** and **19b**) or NaH (**19c-e**) in DMF. The generated *O*-thiocarbamates **20a-e** were subjected to an intramolecular aryl-group migration (Newman-Kwart rearrangement) induced by microwave irradiation at high temperature.[46] The methyl ester group and the *S*-thiocarbamate groups of **21a-d** were hydrolyzed contextually by exposure to NaOH, leading to formation of 2-mercapto benzoic acids **22a-d**. In the case of compound **21e**, hydrolysis of the *S*-thiocarbamoyl (-$SCONMe_2$) group failed under different reaction conditions; it was therefore carried along in the synthesis. Substituted benzoic acids **22a-e** were then treated with $SOCl_2$ and the crude, unpurified acyl chlorides **23a-e** thus obtained were reacted with 2-phenylethylamine,

followed by oxidative cyclization with iodine in a one-pot fashion, to give final compounds **24-28**.[47] Compounds **26** and **27** were further elaborated by removing the methoxy group by exposure to boron tribromide in benzene, to yield final products **29** and **30**, respectively.[48]

Synthesis of BTZs bearing a benzylamino side chain is summarized in Scheme 3.

Scheme 3[a]

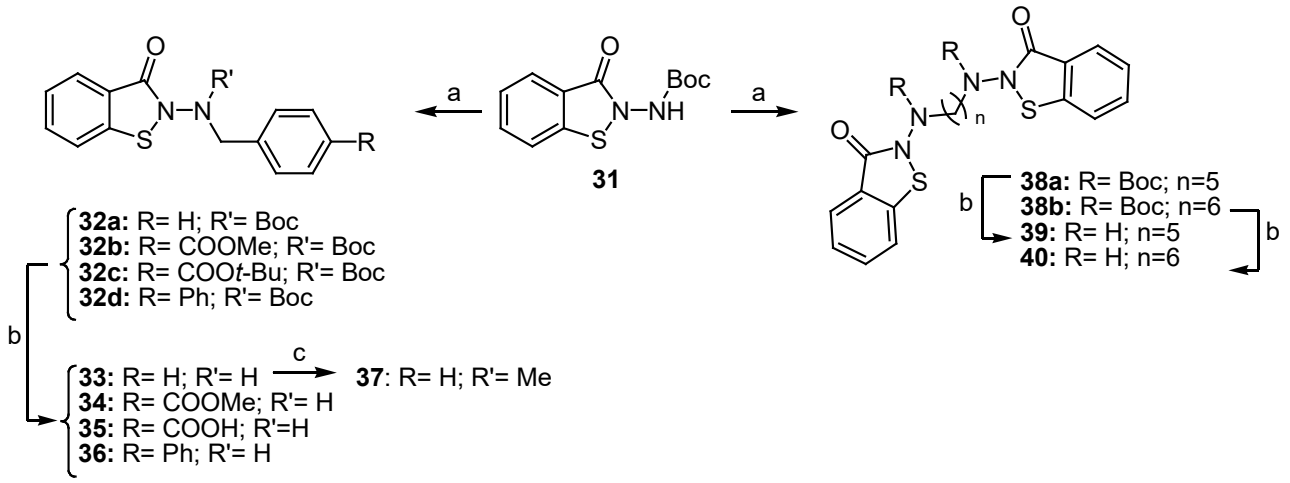

[a]Reagents and conditions: a) KHMDS, alkyl halide, anhydrous DMF, 0 °C to rt, 16 h; b) TFA, DCM, 0 °C to rt, 4 h; c) MeI, imidazole, rt, 16 h.

BTZ **31**[49] was treated with KHMDS and the proper alkyl halide to generate intermediates **32a-d**, from which, upon exposure to an equivolume mixture of trifluoroacetic acid and dichloromethane, the *tert*-butoxy carbonyl protecting group was removed to furnish products **33-36**. Compound **37** was obtained by methylation of **33** with methyl iodide and imidazole. Symmetrically substituted **39** and **40** were obtained from **31** employing the same sequence of alkylation with either 1,5-diiodopentane (**38a**) or 1,6-diiodohexane (**38b**), followed by TFA-induced Boc-deprotection, to yield **39** and **40**, respectively.

Results and discussion

Starting from the potent BTZ derivative **7**,[41] we evaluated different side chains on the nitrogen atom, as well as additional substituents on the BTZ nucleus. The new derivatives were tested for their ability to inhibit recombinant rat MGL overexpressed in *E. coli*. We first focused on the effect exerted by substituents on the nitrogen atom characterized by different size, shape and lipophilicity. Half-maximal inhibitory concentration (IC_{50}) values for BTZs belonging to this first set are reported in Table 1 along with the IC_{50} of reference compound **7**.

Table 1. Inhibition of Purified Recombinant Rat MGL by N-Substituted Benzisothiazolinones.

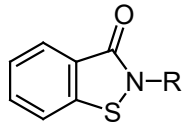

7, **9-11**, **13-16, 33-37**

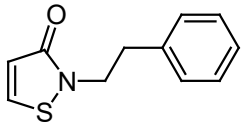

18

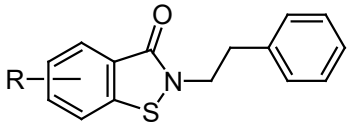

24-30

Compd.	**R**	**IC_{50} (nM)**[a]
7	*n*-octyl	59[b]
9	H	306.5 ± 32.7
10	Me	59.5 ± 5.8
11	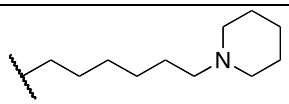	195.2 ± 12.3
13	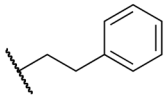	34.1 ± 2.0
14	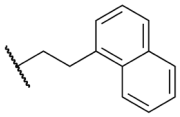	21.8 ± 5.2
15	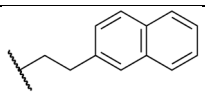	54.2 ± 15.7

16	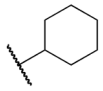	55.5 ± 7.4
18	-	758.6 ± 49.8
24	5-NO_2	163.4 ± 2.8
25	6- NO_2	237.9 ± 10.3
26	5-OMe	568.0 ± 55.3
27	6-OMe	512.2 ± 64.4
28	7-Me	13069.5 ± 523.9
29	5-OH	135.0 ± 3.8
30	6-OH	2547.0 ± 879.7
33	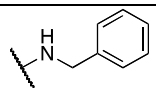	19.5 ± 0.8
34	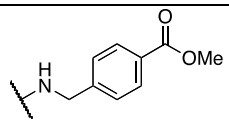	93.9 ± 5.5
35	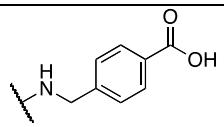	277.7 ± 1.9
36	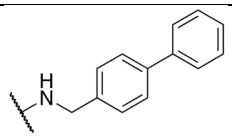	322.1 ± 18.7
37	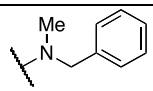	189.4 ± 39.7

[a]IC_{50} values were calculated from dose-response inhibition curves of 2-OG hydrolysis, on cell homogenates of HeLa cells expressing recombinant rat MGL, and 10 min pre-incubation with test compound.[22,71] Results are expressed as mean ± SEM (n = 3-4). [b]Ref.41.

The flexible octyl chain of BTZ **7** was initially replaced with more rigid substituents, as in compounds **14**, **15** and **16** in which the naphthyl-ethyl chains and the cyclohexyl ring appear to be

well tolerated. Size reduction, obtained with a methyl (**10**) or a phenylethyl (**13**) group on the BTZ nitrogen atom, allowed to maintain the same level of inhibitory potency, suggesting that the enzyme can tolerate broad changes in steric bulk and lipophilicity of the *N*-side chain. By contrast, more hydrophilic compounds, such as the piperidino-hexyl derivative **11** or the unsubstituted BTZ **9**, were characterized by a significant reduction of their inhibitory potency. The absence of a substituent on the nitrogen atom in compound **9** allows a prototropic equilibrium which might reduce the availability of the reactive amide form of the sulfenamide warhead. The isothiazolinone **18** carrying a phenethyl chain was significantly less potent than its BTZ analog **13**.

We selected the *N*-phenethyl-BTZ scaffold of **13** to investigate the effect of substituents on the benzene portion of the bicyclic nucleus. Electron-withdrawing or donating groups were introduced in positions conjugated with the sulfur atom or the carbonyl group, to modulate the reactivity of the sulfenamide warhead. We also evaluated the influence of steric hindrance close to the reactive sulfur atom (compounds **24**-**30** in Table 1). Insertion of substituents on the benzene ring led to a general loss of activity, with no clear influence of the electronic effect on inhibitory potency. In fact, the most potent derivatives **24** and **29** carry an electron-withdrawing and donating substituent, respectively, in position 5. While the nitro group in position 6 (**25**) maintained some potency, the 6-hydroxy substituent (**30**) led to one of the highest drops of activity in this series. Compound **28** was the least potent, highlighting the negative effect exerted by a substituent in position 7, close to the reactive sulfur of the BTZ nucleus. The steric hindrance of the methyl group likely affects the reactivity of BTZ, reducing the rate of nucleophilic substitution by the thiol group of targeted cysteines. The results highlight that structural modulation on the benzene ring influences activity in an unpredictable manner. At the same time, the loss of potency caused by introduction of steric hindrance confirms the important role played by the sulfur atom.

To inform subsequent SAR studies on compound **13**, we examined its interaction with MGL using two complementary approaches: site-directed mutagenesis and LC/MS analysis. First, we generated HeLa cells expressing wild-type rat MGL or MGL mutated on Cys201, Cys208 or Cys201 plus

Cys208. Cell extracts were evaluated for MGL activity using a standard enzyme assay (see Methods for details). The results showed that compound **13** was significantly more potent at inhibiting the wild-type form of MGL than it was at inhibiting mutated forms of the enzyme, with IC_{50} values measured for C201A, C208A and C201/208A mutants of 242.9, 72.6, and 604.7 nM, respectively (IC_{50} = 34.1 nM for wild-type MGL) (Figure 3A). As expected from our previous studies,[41] MGL inhibition by compound **13** was fully reversed upon rapid dilution. By contrast, the non-selective serine-targeting inhibitor MAFP (methyl arachidonyl fluorophosphonate) blocked MGL activity in an irreversible manner (Figure 3B).

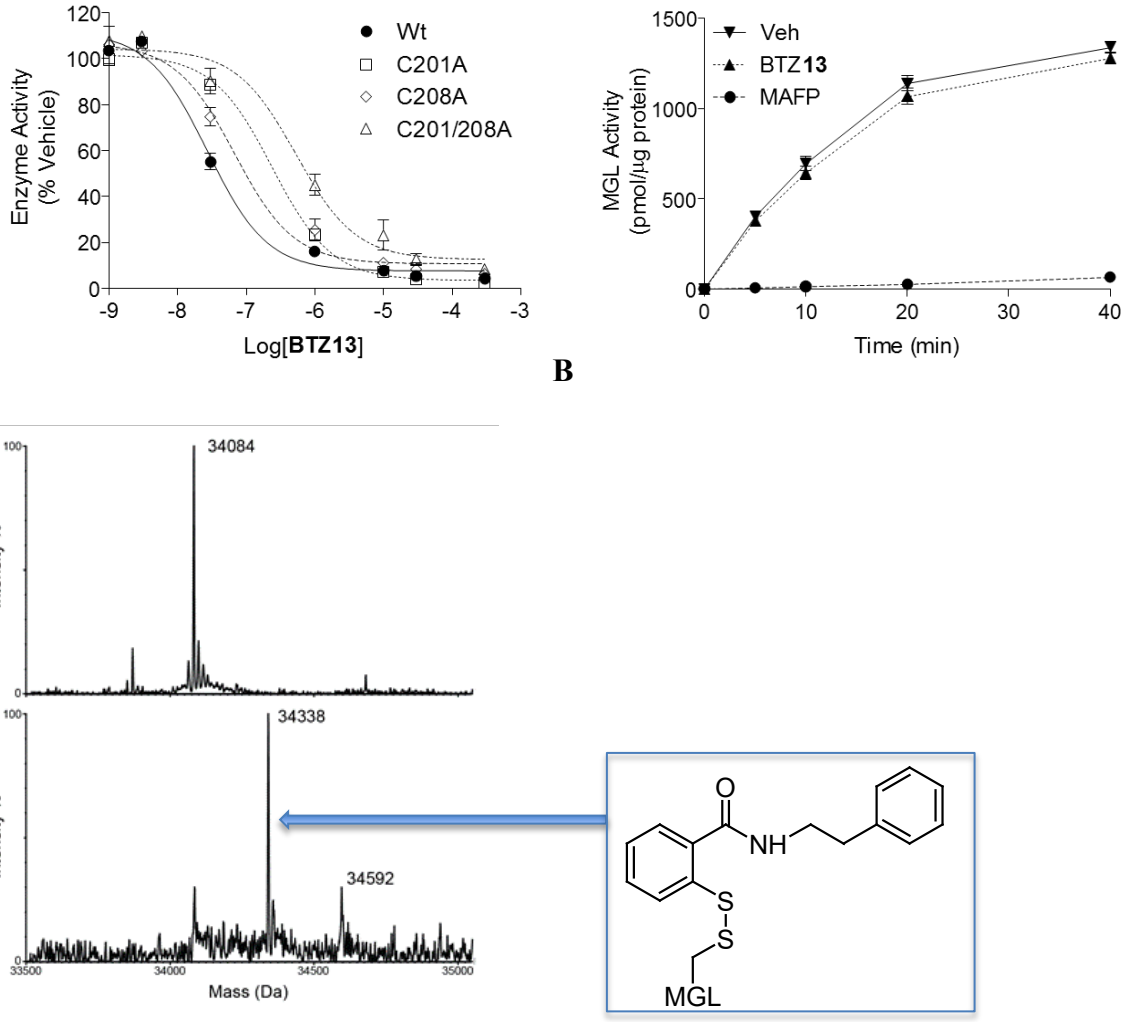

Figure 3. (**A**) Effect of cysteine mutations on rat MGL inhibition by compound **13**. Results are expressed in percentage of control activity (DMSO, final concentration 1%) (mean ± SEM, n = 3-5). Wt = wild type. (**B**) Rapid dilution assays of purified rat MGL in the presence of vehicle (Veh,

DMSO, final concentration 2%), compound **13** (10 μM final concentration), or MAFP (23 nM final concentration). Results are expressed as MGL activity after the indicated incubation time. (**C**) Top: deconvoluted ESI mass spectrum of wild-type human MGL (average mass: 34084 ± 2 Da, n=3). Bottom: deconvoluted ESI mass spectrum of wild-type MGL incubated in the presence of a four-fold molar excess of BTZ **13**. Mass shifts of 254 Da corresponds to the conjugation of one (average mass: 34338 ± 2 Da, n=3) or two (average mass: 34592 ± 2 Da, n=3) molecules of BTZ.

Next, we incubated recombinant wild-type human MGL (Figure S1) in the presence of BTZ **13** (MGL:**13** 1:4 molar ratio, 45 min). The results show that, after exposure to BTZ, the average mass of intact apo-hMGL (34084 ± 2 Da, n=3) was shifted to a value of 34338 ± 2 Da (n=3), compatible with the formation of a 1:1 complex with BTZ **13** (average mass: 255.335) (Figures 3C, S2 and S3). A second signal was also observed at a higher *m/z* (mass-to-charge ratio) (34592 ± 2 Da), which could be attributed to the conjugation of two molecules of BTZ to MGL, but its intensity was ~15-20 % that of the 1:1 MGL-**13** adduct. Then, apo-MGL and MGL incubated with **13** were digested with pepsin to identify specific conjugation site(s). Following apo-MGL incubation, peptides containing three out of the four cysteine residues of human MGL (Cys32, 201 and 242) could be identified (Figure S4A). The short amino acid sequence KVCF, which includes the regulatory Cys208 of MGL, was not covered by peptic peptides despite an overall sequence coverage of 98.7%. In MGL incubations with BTZ **13**, Cys32- and Cys242-containing peptides were identified, as in apo-MGL, but identification of Cys201-containing peptides was not possible indicating modification of this peptide (Figure S4B). In conjunction, a new peptide was identified with an average mass and MS/MS fragmentation pattern compatible with that of the Cys201-containing peptide (aa 193-205 in native human MGL) covalently modified by BTZ (Table S1 and Figure S5). The formation of a reducible disulfide bond between BTZ **13** and the cysteine residue was supported by the fact that application of a reducing agent resulted in the disappearance of the BTZ-

modified peptide, but not of the Cys201-containing peptide in its reduced form (Table S1). These results confirm the mechanism of inhibition of MGL by BTZ **13** via interaction with Cys201, and support a covalent modification of this residue.

To investigate the reactivity of BTZs toward biologically relevant thiols and their ability to promote the chemical transformation of their counterpart, compound **13** was incubated with two equivalents of glutathione (GSH) in physiological conditions (PBS buffer, pH 7.4, 37 °C). The transformations undergone by BTZ **13** are depicted in Figure 4, while the extracted ion chromatograms from the HR-MS full scan analysis are reported in Figure S6. According to reaction A, BTZ **13** reacted with GSH to form the conjugated derivative **41**, mimicking the reaction occurring with cysteines from MGL. Mixed disulfide **41**, upon reaction with another GSH molecule, generated the substituted 2-mercaptobenzamide **42** and oxidized glutathione (GSSG). BTZ **13** could also react (reaction B in Figure 4) with the 2-mercaptobenzamide **42** to generate the symmetric disulfide **43**.

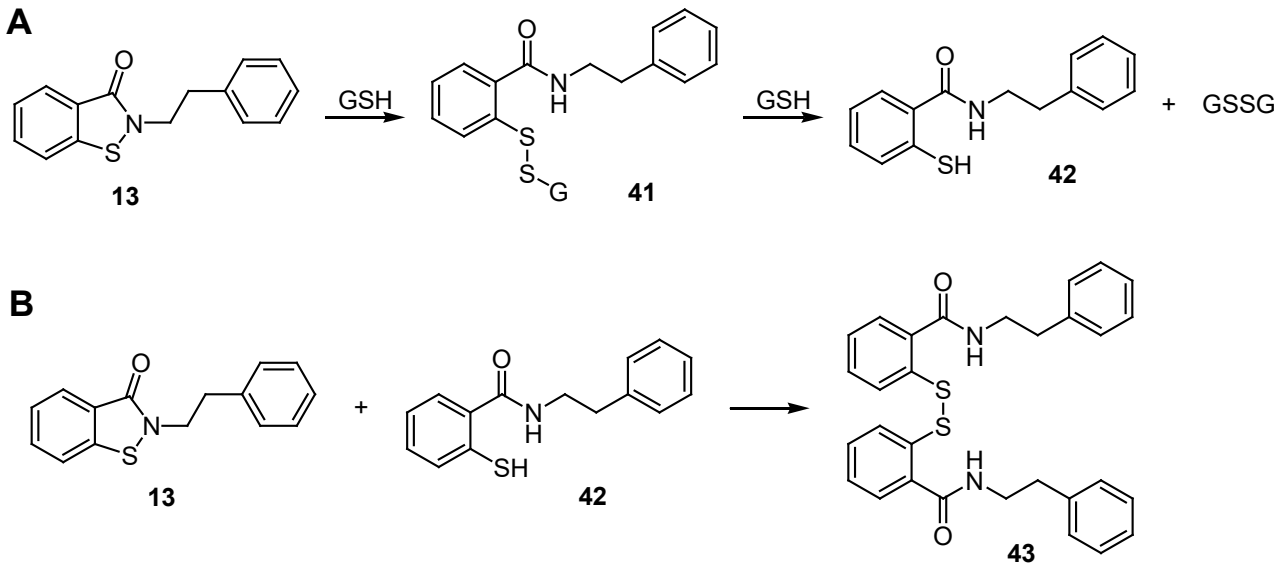

Figure 4. Reactions occurring between BTZ **13** and glutathione (GSH) in solution when present in a 1:2 molar ratio.

Table 2 reports the concentrations of unreacted GSH, oxidized dimeric GSH derivative GSSG, and residual BTZ **13**, and the peak area corresponding to the conjugate between BZT and GSH (**41**,

Figure 4) obtained from a solution of GSH 200 μM and BTZ derivative **13** 100 μM after 60 min of reaction time. BTZ **13** fully reacted with GSH generating the covalent adduct **41** and producing a significant amount of oxidized dimeric GSSG.

Table 2. Reactivity of BTZ **13** with Glutathione.[a]

Compd.	**GSH (μM)**[b]	**GSSG (μM)**[b]	**% oxid.**[c]	**BTZ 13 (μM)**	**Conjugate 41**[d]
13	73.4 ± 4.7	59.3 ± 1.1	61.8	< LOD[e]	721

[a]Data collected at t = 60 min. Starting concentrations: GSH = 200 μM; BTZ **13** = 100 μM. [b]Results are expressed as mean ± SEM (n = 3-4). [c]% of oxidized GSH, calculated as (2[GSSG]/[GSH] + 2[GSSG]) · 100. [d]Value corresponding to peak area of UV chromatogram; a quantification was not possible due to lack of standards. [e]Below limit of detection (LOD).

Supporting the possibility that the interaction of compound **13** with MGL mimics at the functional level hydrogen peroxide-induced sulfenylation, metadynamics simulations revealed that the formation of an adduct between **13** and MGL perturbs the conformational equilibrium between open and closed states of the lid domain, as previously observed for hydrogen peroxide.[40] In fact, both human and rat enzymes are characterized by a dampened activity under oxidative conditions[39,40] and free energy studies provided a plausible description of the mechanism laying behind the oxidative-dependent MGL modulation. Metadynamics simulations suggested that Cys201, reversibly converted into sulfenic acid by oxidative stimuli (e.g., hydrogen peroxide), hampers the recruitment of the substrate from the membrane by affecting the interfacial activation of MGL.[40] To test if BTZ derivatives might modulate MGL through a similar mechanism, we performed well-tempered (wt) metadynamics simulations of human MGL modeled with Cys201 covalently modified by compound **13**, in the presence of a membrane model. The Collective Variables (CV1 and CV2) selected to drive the transition between the open and closed states of the

lid domain were distances between the centers of mass of Cα of residues lining the rims of the lid domain (see Methods for details). This region, representing a membrane-related hydrophobic gate that shapes the active site access channel of the substrate, is stabilized in an open conformation in presence of a membrane model, allowing the recruitment of 2-AG from the membrane.[40] The free energy surface (FES) profile obtained for MGL covalently bound to BTZ **13** revealed only one energy minimum corresponding to the closed state characterized by a reduced distance between the lid domain rims, driven by the simultaneous reduction of CV1 and CV2 values (Figure 5). These results suggest that, similarly to what had been observed for the sulfenylated model of the enzyme,[40] modification of Cys201 through covalent interaction with compound **13** hampers catalytic activity by promoting the closure of the active site access channel.

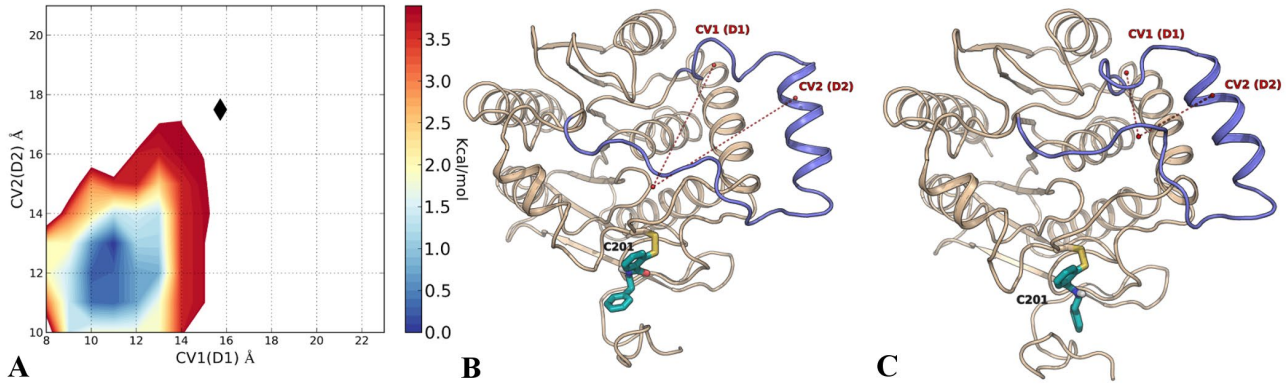

Figure 5. Well-tempered metadynamics simulation of human MGL (PDB 3HJU) with Cys201 covalently bound to BTZ **13**. (A) Free energy surface. A black diamond marks CV1 and CV2 values assumed by the system in its open conformation, measured in the crystal structure 3HJU and corresponding to the starting structure of the metadynamics simulation. (B) Starting conformation of wt metadynamics simulations. Compound **13** covalently bound to Cys201 is represented with green carbons. The rims of the lid domain are depicted with purple cartoons. (C) A conformation corresponding to the free energy minimum of the metadynamics simulation, showing a marked decrease of both CV values and thus a reduced distance between the rims of the lid domain.

Having established that **13** binds to Cys201, but not to active-site Cys242 or peripheral Cys32, we carried out a series of covalent docking studies to generate novel hypotheses about the nature of the interaction between **13** and MGL (Figure 6). A crystal structure of human MGL in which the lid domain is in an open conformation (pdb 3HJU) was used for covalent docking. We modelled the formation of a disulfide adduct between the BTZ derivative and the thiol group of Cys201, with concomitant opening of the isothiazolinone ring and generation of a benzamide derivative. Analysis of docking solutions suggests the existence of four potential strategies for BTZ recognition by MGL (Figure 6A): the formation of i) a hydrogen bond with the carbonyl group of Pro198, as occurring for BTZ **13**; ii) polar interactions with Arg87; iii) hydrophobic interactions with the lipophilic residues surrounding Cys201; and iv) a possible bidentate interaction with both Cys201 and Cys208.

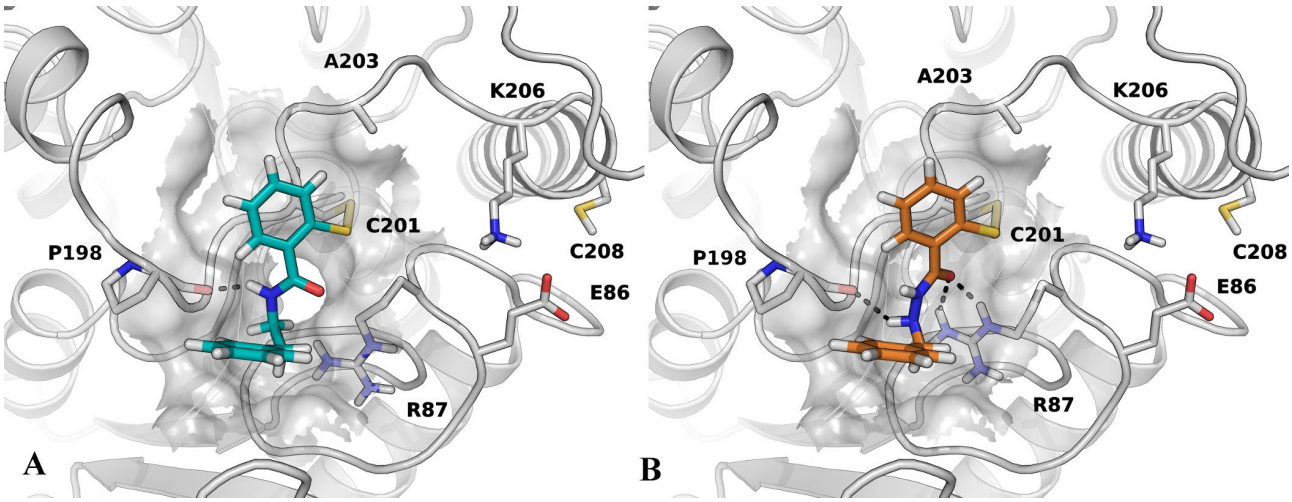

Figure 6. Covalent docking of BTZ **13** (panel A) and **33** (panel B) on Cys201 of human MGL (PDB 3HJU). The molecular surface of MGL in the proximity of the bound ligand is represented in gray. Dashed lines indicate hydrogen bonds.

Following these indications, we synthesized **33**-**37** (Table 1). Replacement of the phenethyl chain on the BTZ nitrogen with a benzylamino group (**33**) resulted in a small but significant improvement in potency. Compound **33** forms a hydrogen bond between the NH group from the benzylamino

side chain and the backbone carbonyl of Pro198, undertaking an additional polar interaction with Arg87 (Figure 6B). Consistently with a role in the recognition event by MGL, methylation of the benzylamino nitrogen significantly reduced potency measured for compound **37**. Attempts to establish additional interactions with polar amino acids (e.g., Arg87) or with the hydrophobic surroundings of Cys201 were performed by inserting suitable substituents on the para position of the benzylamino side chain. However, these structural modifications did not improve potency: indeed, inhibitory potency was maintained in derivative **34**, but was progressively decreased in compounds **35** and **36**.

Docking simulations also highlighted the possibility to accommodate the covalent adducts within the region spanning from Cys201 to Cys208. This observation, coupled with the results of mutagenesis and LC/MS studies, which suggested the participation of both Cys201 and Cys208 to the covalent interaction with BTZs, prompted us to design compounds able to interact with both regulatory cysteines. Based on this premise, we performed an induced fit docking (IFD) study for symmetric BTZ derivatives based on the scaffold of inhibitor **33**, looking for the optimal linker length between the two reactive portions. The results of the IFD study are represented in Figure 7 for compound **39**. The flexible 5-methylene chain occupies the region between Cys201 and Cys208, while the sulfur atoms of the BTZ rings are close to the thiol groups of the two cysteine residues.

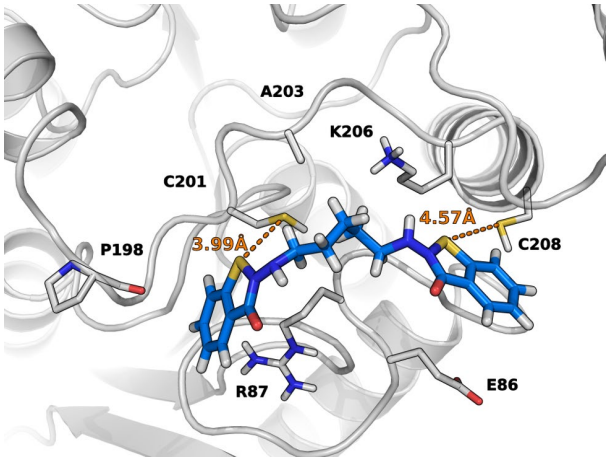

Figure 7. IFD solution obtained for compound **39** spanning the region from Cys201 to Cys208 of human MGL (PDB 3HJU); orange dashes indicate the distance between the sulfur atoms of the benzisothiazolinone rings and those of Cys201 and Cys208.

Compounds **39** and **40**, with a 5- and 6-carbon polymethylene chain, respectively, showed significant MGL inhibitory potencies, with IC_{50} values of approximately 20 nM (Table 3). Mutagenesis data for the most potent BTZ derivatives highlight that inhibitory activity was significantly decreased when Cys201 or Cys208 were mutated to alanine, supporting the involvement of these residues in the inhibitory mechanism (Table 3). Inhibitory potency was further reduced when both cysteines were mutated. This behavior is consistent with a cooperative interaction between the two cysteines, and reproduces what has been previously observed after treatment of MGL with hydrogen peroxide. In fact, hydrogen peroxide oxidized both Cys201 and Cys208, leading to a reduction of MGL activity, impairment of 2-AG degradation and enhancement of 2-AG-mediated signaling in brain neurons.[39] IC_{50} values measured for compounds **39** and **40** in the presence of the C201&208A mutation were twice as high as those of the monomeric derivatives **13** and **33**, supporting a preferential interaction of symmetrical compounds with these two residues.

Table 3. Inhibition of Purified Recombinant Rat MGL with Mutation of Cys201 and Cys208.

Compd.	**Structure**	**IC_{50} (nM)**[a]			
		Wild type	**C201A**	**C208A**	**C201&208A**
13	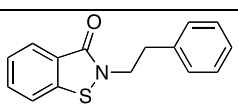	34.1 ± 2.0	242.9 ± 18.0	72.6 ± 30.3	604.7 ± 10.2
33	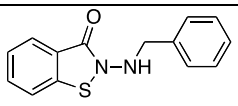	19.5 ± 0.8	54.4 ± 4.1	44.9 ± 8.7	782.0 ± 77.5
39	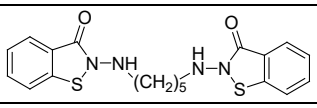	11.5 ± 1.5	229.8 ± 69.0	219.8 ± 33.9	1460.7 ± 465.0

40	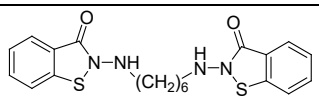	16.8 ± 0.4	114.3 ± 8.9	82.7 ± 11.6	2079.6 ± 40.0

[a]Results are expressed as mean ± SEM (n = 3-4).

Next, we asked whether cysteine-targeting probes such as BTZs might inhibit MGL activity and increase 2-AG levels in intact biological systems. First, we incubated Neuro-2a cells in cultures with hydrogen peroxide, and assessed cellular damage by evaluating lactate dehydrogenase (LDH) release into the culture medium (Figure 8A). For these experiments, we selected an extracellular concentration of hydrogen peroxide (300 μM) that was expected to yield intracellular hydrogen peroxide levels of approximately 30 μM, or three times the IC_{50} of hydrogen peroxide for MGL.[39] Hydrogen peroxide produced significant cellular toxicity, and this effect was heightened by CB_1 cannabinoid receptor blockade with the selective inverse agonist rimonabant, but not by CB_2 blockade with the selective antagonist AM630. This result is consistent with the protective action exerted by CB_1 receptor activation on oxidative damage.[50,51] LDH release was reduced by treatment with the irreversible MGL inhibitor JZL184 (1 μM) and the same effect was produced by BTZ **13** (1 μM). The reduction of hydrogen peroxide toxicity produced by compound **13** or JZL184 was prevented by concomitant application of the CB_1 antagonist rimonabant.

We then assessed the systemic availability of compound **13** following administration of a single 10 mg/kg dose (i.p.) in mice. Maximal plasma levels were reached 15 min after dosing and rapidly declined thereafter (Figure 8B). A similar profile was observed in brain (Figure 8C), though access to this organ was clearly limited (brain/plasma ratio ≈ 4.5%). In a parallel experiment, we determined the ability of **13** (10 mg/kg, i.p.) to impair brain 2-AG degradation. LC/MS analyses showed that 2-AG levels were increased in mice treated with the inhibitor, an effect that was statistically detectable 2 h after administration (Figure 8D). The temporal discrepancy between 2-

AG accumulation (maximal at 2 h) and brain levels of **13** (maximal at 15 min) may be accounted for by slow accumulation of 2-AG in the face of persistent MGL inhibition by compound **13**.

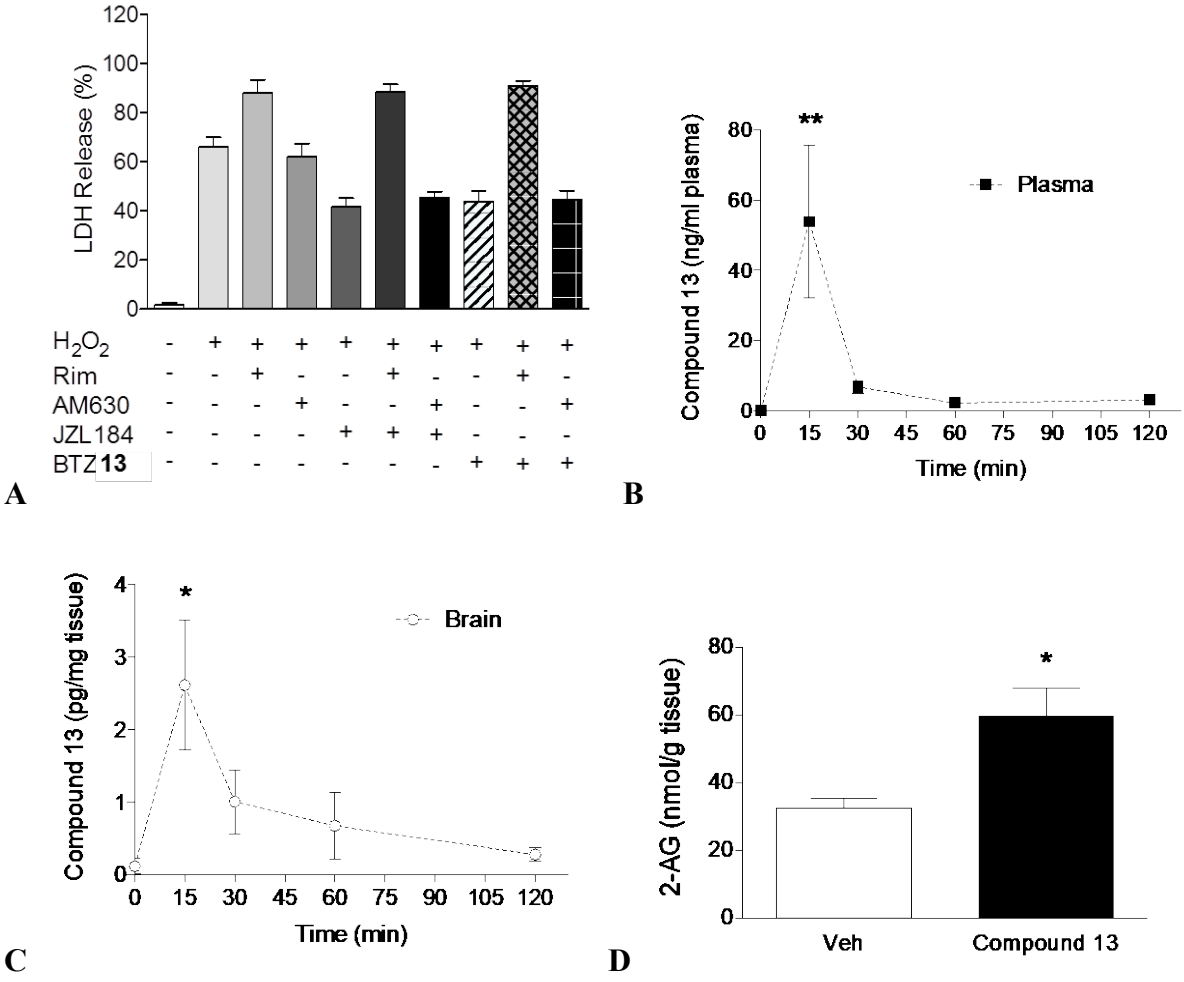

Figure 8. (**A**) Effects of H_2O_2 (300 μM), alone or combined with CB_1 antagonist rimonabant (Rim), CB_2 antagonist AM630, MGL inhibitor JZL184 (1 μM) or compound **13** (1 μM), on lactate dehydrogenase (LDH) release in Neuro-2a cells. (**B**) and (**C**) Plasma and brain concentrations of compound **13** after administration of 10 mg/kg to mice. *P<0.05 and **P<0.01 by two-tailed Student's *t* test or one-way ANOVA followed by Dunnett's multiple comparison test. (**D**) Effect of compound **13** (10 mg/kg) on 2-AG levels in mice brain 2 h after i.p. injection.

Finally, we investigated the interactions of compound **13** with a select series of potential off-targets. We first tested whether the compound interacts (either as an agonist or an antagonist) with proteins that feature free cysteines on their molecular surface, such as the transient receptor potential cation

channel subfamily A member 1 (TRPA1)[52,53] and the transient receptor potential cation channel subfamily V member 1 (vanilloid receptor, TRPV1).[54] Table 4 reports % activation and inactivation of human TRPA1 and TRPV1 channels produced by compound **13** at different concentrations in an aequorin-based calcium mobilization assay. The compound showed little or no agonist activity on either channel, and marginal antagonist activity on TRPA1 at concentrations >500 nM (25 times greater than those needed to block MGL).

Table 4. Activation and Inhibition of Human TRPA1 and TRPV1 Ion Channels Exerted by Compound **13** and Binding Affinity of Compound **13** for rat cannabinoid receptors.[a]

Conc (nM)	**hTRPA1**	**hTRPV1**		**rCB_1**	**rCB_2**
Agonist assay	***% activation***				
100	-0.15	0.21			
1000	1.74	0.59			
2000	19.30	1.78			
Antagonist assay	***% inhibition***		***Binding assay***[b]	***% bound radioligand***	
50	-22.76	-9.82		100.59	100.41
500	55.97	-10.75		106.32	119.67
1000	71.54	8.55		91.76	95.21

[a]Each concentration was tested in duplicate. [b]Reported is the % bound radioligand in the presence of compound **13** at the specified concentration.

To determine if compound **13** can affect the activity of other components of the endocannabinoid system, we tested its affinity for rat CB_1 and CB_2 cannabinoid receptors, as well as the ability to inhibit various enzymes involved in the metabolism of 2-AG or anandamide, i.e.: i. rat diglyceride lipase-α (DGL-α), the serine hydrolase that catalyzes mGluR5-operated 2-AG formation in spines;[55,56] ii. mouse alpha/beta hydrolase domain containing 6 (ABHD6);[57] and iii. rat fatty acid

amide hydrolase (FAAH).[58] Compound **13** was devoid of significant binding at either rat CB_1 or CB_2 receptors at the concentrations tested (50, 500 and 1000 nM) (Table 4). Figure 9 depicts the inhibition curves of rat DGL-α (left panel) and rat FAAH (middle panel) and the effect of compound **13** on mouse ABHD6-catalyzed 2-AG hydrolysis (right panel). Compound **13** had no effect on DGL-α activity at any of the concentrations tested and only modestly inhibited ABHD6 and FAAH, with IC_{50} values of 3.58 and 9.38 μM, respectively.

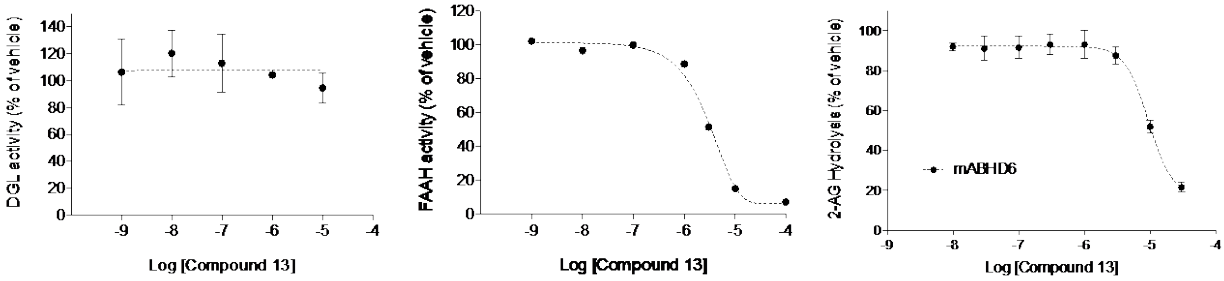

Figure 9. Effects of compound **13** on diglyceride lipase (left) and FAAH (center) activities from rat brain homogenate, and mouse ABHD6 activity from ABHD6-expressing HEK cell lysate (right). Results are expressed as mean ± SEM; n = 3-6, with each assay was performed in duplicate.

Conclusions

We describe a series of BTZ derivatives that act as allosteric inhibitors of MGL activity by covalently and reversibly interacting with Cys201 and Cys208, two regulatory cysteines located in close proximity of the lid domain of this serine hydrolase. Metadynamics simulations revealed that BTZ-modified MGL tends to assume a closed conformation that hampers substrate recruitment into the enzyme active site. Focused SAR investigations led to the potent derivative **13**, which showed neuroprotective activity *in vitro* and was able to elevate brain 2-AG levels *in vivo*. Pharmacokinetic profiling in mice shows a rapid access of the compound to plasma and brain after i.p.

administration, though further work is needed to improve plasma life-time and brain access for this class of agents.

BTZ derivatives act as general cysteine-targeting agents and have been shown to covalently modify multiple enzymes.[59,60,61] Nevertheless, we found that compound **13** does not significantly interfere with the activity of two cysteine-rich proteins (TRPAV1 and TRPA1) and of several key components of the endocannabinoid system (DGL-α, ABHD-6, FAAH). Four additional lines of evidence indicate that **13** interacts selectively with MGL: i) its high inhibitory potency; ii) mutagenesis experiments highlighting the involvement of Cys201 and Cys208 in its inhibitory mechanism; iii) mass spectrometry data indicating interaction of **13** with Cys201, but not other cysteines (Cys32 and Cys242); iv) SAR explorations clarifying the importance of lipophilic substituents for productive interactions with the environment surrounding the modulatory cysteine residues.

In sum, our results show that it is possible to develop small-molecule allosteric MGL inhibitors that recapitulate the ability of the intracellular second messenger, hydrogen peroxide, to modulate MGL activity and enhance 2-AG mediated signaling. It is tempting to speculate that a similar strategy might be deployed to modify the activity of other proteins that contain modulatory cysteines, such as peroxiredoxins and NRF2.

Experimental section

Chemistry

All chemicals were used as received unless stated otherwise. All reactions were performed under a steady overpressure of nitrogen delivered through a balloon. Tetrahydrofuran was distilled over sodium/benzophenone prior to use. Anhydrous solvents such as dichloromethane, *N,N*-dimethylformamide, toluene and acetonitrile were directly purchased from an appropriate vendor,

and were supplied stored over 3 Å molecular sieves and packed under Ar. They were subsequently manipulated by syringe under a steady pressure of nitrogen. Column chromatography was performed on silica gel 60 (0.040-0.063 mm) under forced flow of the appropriate solvent mixtures. TLC analysis was conducted on HPTLC aluminum sheets (Sigma-Aldrich, silica gel 60, F_{254}), compounds were visualized by UV absorption (245 nm) and/or by dipping in a solution of $(NH_4)_6Mo_7O_{24}\cdot 4\ H_2O$ 25 g/L and $(NH_4)_4Ce(SO_4)_4\cdot 2\ H_2O$ 10 g/L, in 1 L of 10% aqueous H_2SO_4. Microwave reactions were conducted using a CEM Discover synthesis unit (CEM Corp., Matthews, NC). Melting points were not corrected and were determined with a Gallenkamp melting point apparatus. ^{1}H-NMR spectra were recorded with a Bruker AV 300 or 400 MHz. Chemical shifts (δ scale) are reported in parts per million (ppm), referenced to TMS or the residual solvent signal. ^{1}H-NMR spectra are reported in the following order: multiplicity, number of protons and approximate coupling constant (*J* value) in hertz (Hz); signals were characterized as s (singlet), d (doublet), dd (doublet of doublets), t (triplet), dt (doublet of triplets), q (quartet), m (multiplet), bs (broad signal). Mass spectra were recorded on an Applied Biosystem API-150 EX system spectrometer with an ESI or an APCI interface. Compound **17** was synthesized according to literature methods.[45] Compound **9** was purchased from Sigma-Aldrich and checked for purity by elemental analysis (Calc. for C_7H_5NOS: C, 55.61; H, 3.33; N, 9.26. Found: C, 55.64; H, 3.21; N, 9.23). Purity of final compounds was analyzed either on a ThermoQuest (Italia) FlashEA1112 Elemental Analyzer for C, H, and N (analyses were within 0.4% of theoretical values) or by analytical high performance liquid chromatography (HPLC) employing a Shimadzu HPLC gradient system (Shimadzu Corp., Kyoto, Japan) equipped with two LC-10AD solvent delivery modules, a Rheodyne 7125 sample injector and a SPD-10A UV-VIS detector. Prior to analysis, samples were prepared in MeOH at a final concentration of 0.1 mg/mL. Chromatographic separation occurred on a Supelco Discovery C_{18} column (150 X 4.6 mm, 5 μm particle size) by gradient elution. Flow rate was 1 mL/min and injected volume was 10 μL. Solvent A was methanol and Solvent B was water both additioned of 0.1% v/v formic acid. Gradient conditions A: t(0 min): 55% A: 45% B; t(15 min): 95% A: 5% B;

t(17 min): 95% A: 5% B; returning to initial conditions after 1 min were employed for all compounds. Purity results are presented as *t*R (min) and relative chemical purity (%). All tested compounds were > 95% pure.

2-Methylbenzo[*d*]isothiazol-3(2*H*)-one 10. To a stirred solution of benzo[*d*]isothiazol-3(2*H*)-one **9** (61.2 mg, 0.39 mmol) in MeCN (2 ml), K_2CO_3 (54.1 mg, 0.39 mmol) was added and the resulting suspension is stirred for 10 min under nitrogen atmosphere. Iodomethane (100 μL, 1.57 mmol) was dropwise added over 5 min and the resulting mixture was stirred for 16 h. The volatile material is removed by distillation under reduced pressure and the crude product is purified by FC (SiO_2, Et_2O) to give 26.3 mg (40%) of the expected product **10** a as white waxy solid. Analytical data agree with those reported.[62] LC-UV *t*R purity: 4.36 min – 98.7%.

2-(6-Chlorohexaneyl)benzo[*d*]isothiazol-3(2*H*)-one 10a. To a stirred solution of benzo[*d*]isothiazol-3(2*H*)-one **9** (100.4 mg 0.66 mmol) in CH_3CN (2 mL), K_2CO_3 (91.7 mg, 0.67 mmol) was added and the resulting suspension was stirred for 10 min under nitrogen atmosphere. 1-Chloro-6-iodohexane (1.0 mL, 6.6 mmol) was dropwise added over 5 min and the resulting mixture was stirred for 18 h and then refluxed for 1 h. The solvent was removed by distillation under reduced pressure and the crude was purified by FC (SiO_2, AcOEt/Hexane 50:50) to give 66.7 mg of the expected product **10a** as colorless oil (37%). ^{1}H-NMR (300 MHz, $CDCl_3$) δ: 8.03 (d, *J*= 7.9 Hz, 1H); 7.49-7.42 (m, 1H); 7.40 (td, *J* = 8.0, 1.3 Hz, 1H); 3.90 (t, *J* = 7.1 Hz, 2H); 3.52 (t, *J* = 6.6 Hz, 2H); 1.78 (m, 4H); 1.51 (m, 4H).

2-(6-(Piperidin-1-yl)hexaneyl)benzo[*d*]isothiazol-3(2*H*)-one 11. In an amber glass vial with seal, piperidine (58 μL, 0.6 mmol) was added to a stirred suspension of K_2CO_3 (169.0 mg, 1.22 mmol), KI (8.0 mg, 0.05 mmol) and **10a** (66.4 mg, 0.25 mmol) in anhydrous DMF (1.0 mL). Upon completion of addition, the reaction mixture was heated to 110 °C and stirred under nitrogen

atmosphere for 6 h. The volatiles were removed under reduced pressure and the crude reaction mixture was diluted with AcOEt, the salts removed by filtration and the solvent evaporated under reduced pressure. FC (SiO_2, DCM/MeOH 95:5) furnished 33.0 mg (41%) of **11** as colorless oil. ^{1}H-NMR (300 MHz, $CDCl_3$) δ: 8.00 (d, *J* = 7.9 Hz, 1H); 7.61-7-52 (m, 2H); 7.38 (m, 1H); 3.87 (t, *J* = 7.3 Hz, 2H); 2.35 (bs, 4H); 2.27 (t, *J* = 7.8 Hz, 2H); 1.75 (quintet, *J* = 7.1 Hz, 2H); 1.61-1.32 (m, 12H). MS-APCI: Calc. for $C_{18}H_{26}N_2OS$: 318.2, Found: 319.5 $[M+H]^+$. Anal. Calc. for $C_{18}H_{26}N_2OS$: C, 67.88; H, 8.23; N, 8.80; Found: C, 67.49; H, 8.15; N, 8.63.

2-(Chlorocarbonyl)phenyl hypochlorothioite 12. To a suspension of 2,2'-dithiosalicyclic acid (2.02 g, 6.58 mmol) in toluene (10 mL) at 0 °C, thionyl chloride (1.65 g, 13.83 mmol) and a catalytic amount of DMF (few drops) were added. The mixture was heated at 75 °C for 18 h and the dark solution thus obtained was finally cooled to 0 °C. The crystals that separated were collected by filtration, rinsed with cold hexane and air-dried to afford 1.60 g (70%) of 2,2'-dithiobisbenzoyl chloride. The crude chloride was suspended at 0 °C in DCM (8.5 mL), and excess Cl_2 was allowed to bubble through the suspension. When a perfectly homogeneous solution is obtained, the stream of chlorine was stopped and the solution of crude **12** was used as obtained.[44]

General method A. To a stirred solution of the amine (1.5 equiv) and anhydrous TEA (4.8 equiv) in anhydrous DCM, a solution of **12** in anhydrous DCM was added dropwise over 2 min. The reaction mixture was stirred at rt under nitrogen atmosphere for 16 h. The volatile components were removed under reduced pressure, the residue was taken up with AcOEt and the resulting mixture was washed sequentially with $NaHCO_3$ saturated aqueous solution, 0.1M HCl aqueous solution and brine. The organic phase was dried over Na_2SO_4 and the solvent removed under reduced pressure.

2-Phenylethylbenzo[*d*]isothiazol-3(2*H*)-one 13. According to method A, after purification by FC (SiO_2 Hexane/AcOEt 70:30) and crystallization from *n*-hexane, **13** (16.1 mg, 11%) was obtained as

pale yellow crystals. Analytical data agree with those reported.[63] LC-UV purity *t*R: 12.1 min – 99.8%.

2-(2-(Naphthalen-1-yl)ethyl)benzo[d]isothiazol-3(2H)-one 14. According to method A, after purification by FC (SiO_2 Hexane/AcOEt 70:30) and crystallization from *n*-hexane, **14** (25 mg, 14%) was obtained as pale yellow crystals. ^{1}H-NMR (300 MHz, $CDCl_3$) δ: 8.25 (d, *J* = 8.4 Hz, 1H); 8.07 (d, *J* = 7.8 Hz, 1H); 7.88 (d, *J* = 7.8 Hz, 1H); 7.78 (t, *J* = 4.5 Hz, 1H); 7.63-7.39 (m, 7H); 4.22 (t, *J* = 7.8 Hz, 2H); 3.54 (t, *J*=7.8 Hz, 2H). MS-APCI: Calc. for $C_{19}H_{15}NOS$: 305.08, Found: 306.2 $[M+H]^+$. Anal. Calc. for $C_{19}H_{15}NOS$: C, 74.72; H, 4.95; N, 4.59. Found: C, 74.66; H, 4.98; N, 4.61. mp = 101-102 °C.

2-(2-(Naphthalen-2-yl)ethyl)benzo[*d*]isothiazol-3(2*H*)-one 15. According to method A, after purification by FC (SiO_2 Hexane/AcOEt 70:30) and crystallization from *n*-hexane, **15** (28.7 mg, 16%) was obtained as pale yellow crystals. ^{1}H-NMR (300 MHz, $CDCl_3$) δ: ^{1}H-NMR (300 MHz, $CDCl_3$) δ: 8.04 (d, *J* = 7.8 Hz, 1H); 7.76-7.83 (m, 3H); 7.71 (s, 1H); 7.58 (td, *J* = 8.2, 1.2 Hz, 1H); 7.36-7.50 (m, 5H); 4.23 (t, *J*= 7.2 Hz, 2H); 3.24 (t, *J* = 7.5Hz, 2H). MS-APCI: Calc. for $C_{19}H_{15}NOS$: 305.08, Found: 306.3 $[M+H]^+$. LC-UV purity *t*R: 14.8 min – 99.8%. mp = 114-115 °C.

2-Cyclohexylbenzo[*d*]isothiazol-3(2*H*)-one 16. According to method A, after purification by FC (SiO_2 Hexane/AcOEt 70:30) and crystallization from *n*-hexane, **16** (31.2 mg, 30%) was obtained as pale yellow crystals. Analytical data agree with those reported.[64] Anal. Calc. for $C_{16}H_{15}NOS$: C, 66.92; H, 6.48; N, 6.00; Found: C, 66.68; H, 6.58; N, 5.82.

2-Phenethylisothiazol-3(2*H*)-one 18. A solution of SO_2Cl_2 in anhydrous 1,2-dichloroethane (0.75 M, 4.8 ml, 3.6 mmol) was added dropwise to a 0 °C stirring suspension of 3,3'-disulfanediylbis(*N*-phenethylpropanamide) **17** (500.2 mg, 1.20 mmol) in anhydrous 1,2-dichloroethane (7.0 mL) over 2

h. The solvent was evaporated under reduced pressure and the yellow oily residue was taken up with DCM. The resulting mixture was washed twice with H_2O, dried over anhydrous Na_2SO_4, filtered and concentrated under reduced pressure. The crude product was purified by FC (SiO_2, DCM/Et_2O 98:2 then 90:10) and crystallized from *n*-hexane giving 194.8 mg of desired product **18** as a pale yellow powder (39%). Analytical data agree with those reported.[45] Anal. Calc. for $C_{11}H_{11}NOS$: C, 64.36; H, 5.40; N, 6.82; Found: C, 64.48; H, 5.42; N, 6.84.

General method B. To a solution of **19a-e** and the appropriate base in anhydrous DMF *N,N*-dimethyl thiocarbamoylchloride (1.5 equiv) was quickly added under N_2 atmosphere. The reaction was allowed to proceed for 3 h. The volatile materials were removed under reduced pressure and the residue was dissolved in AcOEt and washed twice with H_2O, diluted HCl and saturated aqueous $NaHCO_3$. The organic phases were collected, dried over Na_2SO_4 and the solvent removed under reduced pressure. The crude product was subjected to flash column chromatography with an appropriate eluent mixture to furnish the purified product.

Methyl 2-((dimethylcarbamothioyl)oxy)-5-nitrobenzoate 20a. Prepared according to general method B, starting from methyl 2-hydroxy-5-nitrobenzoate **19a** (500.0 mg, 2.54 mmol) and using DABCO (341.2 mg, 3.04 mmol) as base. FC (SiO_2, Hexane/AcOEt 80:20) furnishes 498.3 mg of desired product as a yellow powder (yield = 68%). ^{1}H-NMR (300 MHz, $CDCl_3$) δ: 8.86 (d, J = 2.8 Hz, 1H); 8.41 (d, J = 8.9, 2.9 Hz, 1H); 7.29 (d, J = 8.9 Hz, 1H); 3.90 (s, 3H); 3,46 (s, 3H); 3.42 (s, 3H).[65]

Methyl 2-((dimethylcarbamothioyl)oxy)-4-nitrobenzoate 20b. Prepared according to general method B, starting from methyl 2-hydroxy-4-nitrobenzoate **19b** (598.7 mg, 3.05 mmol) and using DABCO (681.0 mg, 6.09 mmol) as base. FC (SiO_2, Hexane/AcOEt 75:25) furnished 396.4 mg of

desired product as a yellow powder (yield = 40%). ^{1}H-NMR (300 MHz, $CDCl_3$) δ: 8.15 (m, 2H); 8.00 (s, 1H); 3.90 (s, 3H); 3.47 (s, 3H); 3.43 (s, 3H).

Methyl 2-((dimethylcarbamothioyl)oxy)-5-methoxybenzoate 20c. Prepared according to general method B, starting from methyl 2-hydroxy-5-methoxybenzoate **19c** (2003.1 mg, 10.9 mmol) and using NaH (60% dispersion in mineral oil, 526.7 mg, 13.2 mmol) as base. The residue was triturated with Et_2O to give 1830.6 mg of desired product as a white powder (yield = 65%). ^{1}H-NMR (400 MHz, $CDCl_3$) δ: 7.51 (d, *J* = 3.0 Hz, 1H); 7.11 (dd, *J* = 8.8, 3.0 Hz, 1H); 7.05 (d, *J* = 8.8 Hz, 1H); 3.86 (s, 6H); 3.49 (s, 3H); 3.41 (s, 3H).

Methyl 2-((dimethylcarbamothioyl)oxy)-4-methoxybenzoate 20d. Prepared according to general method B, starting from methyl 2-hydroxy-4-methoxybenzoate **19d** (2002.7 mg, 10.9 mmol) and using NaH (60% dispersion in mineral oil, 525.9 mg, 13.2 mmol) as base. The residue was triturated with Et_2O to give 1712.0 mg of desired product as a white powder (yield = 60%). ^{1}H-NMR (300 MHz, $CDCl_3$) δ: 7.96 (d, *J* = 8.8 Hz, 1H); 6.82 (dd, *J* = 8.8, 2.6 Hz, 1H); 6.62 (d, *J* = 2.5 Hz, 1H); 3.85 (s, 3H); 3.80 (s, 3H); 3.47 (s, 3H); 3.39 (s, 3H).[66]

Methyl 2-((dimethylcarbamothioyl)oxy)-3-methylbenzoate 20e: Prepared according to general method B, starting from methyl 2-hydroxy-3-methylbenzoate **19e** (1997.3 mg, 12.0 mmol) and using NaH (60% dispersion in mineral oil, 525.4 mg, 13.2 mmol) as base. The residue was purified by FC (SiO_2, Hexane/AcOEt 90:10) to give 711.5 mg of desired product as a yellow powder (yield = 55%). ^{1}H-NMR (300 MHz, $CDCl_3$) δ: 7.80 (dd, *J* = 7.8, 1.3 Hz, 1H); 7.38 (dd, *J* = 6.9, 1.0, 1H); 7.16 (t, *J* = 7.7, 1H) 3.78 (s, 3H); 3.42 (s, 3H); 3.35 (s, 3H); 2.21 (s, 3H).

General method C. The substituted 2-dimethylthiocarbamoyl benzoates **20a-e** were mixed with diphenylether in a microwave reaction vessel, without sealing. The mixture was heated to 250 °C

with the aid of a microwave reactor (300 W), for the required time. When TLC analysis showed complete consumption of the starting material, the mixture was allowed to cool while keeping the temperature above the melting point of diphenylether. The liquid mixture was loaded on top of a SiO_2 column packed with hexanes/AcOEt = 3/2 and rapidly eluted with the same mixture to remove diphenyl ether. Further elution allowed collection of fractions containing the products, which were evaporated and subjected to flash column chromatography with an appropriate eluent mixture to furnish the purified product.

Methyl 2-((dimethylcarbamoyl)thio)-5-nitrobenzoate 21a. According to general method C, compound **20a** (640.3 mg, 2.25 mmol) was reacted for 1 min and purified by FC (SiO_2, Hexane/AcOEt 60:40) giving 489.9 mg of desired product as a yellow solid (yield = 78%). ^{1}H-NMR (300 MHz, $CDCl_3$) δ: 8.73 (d, *J* = 2.6 Hz, 1H); 8.28 (dd, *J* = 8.7, 2.6 Hz, 1H); 7.84 (d, *J* = 8.7 Hz, 1H); 3.95 (s, 3H); 3.15 (bs, 3H); 3.05 (bs, 3H).

Methyl 2-((dimethylcarbamoyl)thio)-4-nitrobenzoate 21b. According to general method C, compound **20b** (396.4 mg, 1.39 mmol) was reacted for 20 min and purified by FC (SiO_2, Hexane/AcOEt 70:30) giving 319.0 mg of desired product as a yellow solid (yield = 80%), ^{1}H-NMR (300 MHz, $CDCl_3$) δ: 8.46 (d, *J* = 2.1 Hz, 1H); 8.23 (dd, *J* = 8.6, 2.2 Hz, 1H); 8.00 (d, *J* = 8.6 Hz, 1H) 3.93 (s, 3H); 3.15 (s, 3H); 3.04 (s, 3H).

Methyl 2-((dimethylcarbamoyl)thio)-5-methoxybenzoate 21c. According to general method C, compound **20c** (200.1 mg, 0.70 mmol) was reacted for 20 min and purified by FC (SiO_2, Hexane/AcOEt 60:40) giving 190.1 mg of desired product as a yellow oil (yield = 95%). ^{1}H-NMR (300 MHz, $CDCl_3$) δ: 7.40 (d, *J* = 8.6 Hz, 1H); 7.32 (d, *J* = 2.9 Hz, 1H); 6.93 (dd, *J* = 8.8, 2.9 Hz, 1H); 3.79 (s, 3H); 3.74 (s, 3H); 2.96 (bs, 6H).

Methyl 2-((dimethylcarbamoyl)thio)-4-methoxybenzoate 21d. According to general method C, compound **20d** (199.7 mg, 0.70 mmol) was reacted for 10 min and purified by FC (SiO_2, Hexane/AcOEt 80:20) giving 190.5 mg of desired product as a yellow oil (yield = 95%). ^{1}H-NMR (400 MHz, $CDCl_3$) δ: 7.78 (d, *J* = 8.7 Hz, 1H); 7.03 (d, *J* = 2.5 Hz, 1H); 6.76 (dd, *J* = 8.7, 2.5 Hz, 1H); 3.69 (s, 3H); 3.66 (s, 3H); 2.94 (bs, 3H); 3.87(bs, 3H).

Methyl 2-((dimethylcarbamoyl)thio)-3-methylbenzoate 21e. According to general method C, compound **20e** (824.8 mg, 3.26 mmol) was reacted for 30 min and purified by FC (SiO_2, Hexane/AcOEt 80:20) giving 735.2 mg of desired product as a yellow oil (yield = 89%). ^{1}H-NMR: (300 MHz, $CDCl_3$) δ: 7.54 (dd, *J* = 7.5, 1.6 Hz , 1H); 8.28 (dd, *J* = 7.6, 1.1 Hz, 1H); 7.29 (d, *J* = 7.6 Hz, 1H) 3.83 (s, 3H); 3.09 (bs, 3H); 2.97 (bs, 3H); 2.43 (s, 3H).[67]

General method D. Intermediates **21a-e** were suspended in a 2:1 MeOH/H_2O mixture, NaOH was added and the reaction was refluxed for 16 h. MeOH was removed under reduced pressure and the mixture was cooled by adding ice water. HCl 1% was added to the solution until a white precipitate appears. The precipitate was filtered off and dried to afford the desired compound used without any further purification.

2-Mercapto-5-nitrobenzoic acid 22a. According to general method D, starting from methyl 2-((dimethylcarbamoyl)thio)-5-nitrobenzoate **21a** (500.3 mg, 1.75 mmol), **22a (**255.3 mg, 73%) was obtained as a yellow powder. ^{1}H-NMR (300 MHz, DMSO-d_6) δ: 8.69 (s, 1H); 8.34 (m, 1H); 8.13 (m, 1H).

2-Mercapto-4-nitrobenzoic acid 22b. According to general method D, starting from methyl 2-((dimethylcarbamoyl)thio)-4-nitrobenzoate **21b** (318.7 mg, 1.12 mmol), **22b (**171.8 mg, 77%) was

obtained as a yellow powder. ^{1}H-NMR (300 MHz, CD_3OD) δ: 8.57 (s, 1H); 8.34 (d, *J* = 8.5 Hz, 1H); 8.13 (d, *J* = 8.6 Hz, 1H).

2-Mercapto-5-methoxybenzoic acid 22c. According to general method D, starting from methyl 2-((dimethylcarbamoyl)thio)-5-methoxybenzoate **21c** (1701.8 mg, 6.31 mmol), **22c (**603.2 mg, 52%) was obtained as a white powder. Analytical data agree with those reported.[68]

2-Mercapto-4-methoxybenzoic acid 22d: According to general method D, starting from methyl 2-((dimethylcarbamoyl)thio)-4-methoxybenzoate **21d** (1605.4 g, 5.96 mmol), **22d** (1010.0 mg, 92%) was obtained as a white powder. Analytical data agree with those reported.[66]

2-((Dimethylcarbamoyl)thio)-3-methylbenzoic acid 22e: According to general method D, starting from methyl 2-((dimethylcarbamoyl)thio)-3-methylbenzoate **21e** (734.8 mg, 2.9 mmol), product **22e (**292.7 mg, 60%) was obtained as a white powder. ^{1}H-NMR (300 MHz, D_2O) δ: 7.38 (m, 3H); 3.04 (bs, 3H); 3.04 (bs, 3H); 2.84 (bs, 3H); 2.28 (s, 3H).

General method E. **Preparation of Acyl Chlorides 23a-e**. Compounds **22a-e** were suspended in $SOCl_2$ (15 equiv) and refluxed for 6 h, after which excess thionyl chloride was removed *in vacuo*. The residue was coevaporated twice with anhydrous toluene, and the oily residue was used for the subsequent step without further purification.

General method F. In a two-neck flask, 2-phenyl ethylamine (1.25 equiv) was dissolved in anhydrous THF at 0 °C. Anhydrous TEA (3 equiv) was added to the mixture and a solution of crude acyl chloride **23a-e** (1 equiv) in anhydrous THF was added dropwise over the course of few minutes. The reaction was gently warmed to rt and stirred for 16 h. A solution of I_2 (1.25 equiv)

dissolved in anhydrous THF was then added and the resulting mixture was stirred for further 4 h. The solvent was removed under reduced pressure and the residue was dissolved in AcOEt and washed twice with a phosphate buffer. The organic layer was dried over Na_2SO_4 and the solvent removed under reduced pressure to afford the crude product that was subjected to flash column chromatography with an appropriate eluent mixture and/or to crystallization to furnish the purified product.

5-Nitro-2-phenethylbenzo[*d*]isothiazol-3(2*H*)-one 24. Starting from compound **23a** (279.8 mg, 1.29 mmol), the desired product was obtained as yellow crystals (228.6 mg, 60%) after purification by FC (SiO_2, Hexane/AcOEt 80:20) and crystallization from DCM/*n*-hexane. ^{1}H-NMR (300 MHz, $CDCl_3$) δ: 8.86 (d, *J* = 2.1 Hz, 1H); 8.41 (dd, *J* = 8.8, 2.3 Hz, 1H); 7.62 (d, *J* = 8.8 Hz, 1H); 7.25 (m 4H); 4.15 (t, *J* = 7.1 Hz, 2H); 3.07 (t, *J* = 7.3 Hz, 2H). MS-APCI: Calc. for $C_{15}H_{12}N_2O_3S$: 300.1, Found: 301.3 $[M+H]^+$. LC-UV purity: *t*R 8.45 min - 99.2%. mp = 140 °C.

6-Nitro-2-phenethylbenzo[*d*]isothiazol-3(2*H*)-one 25. Starting from compound **23b** (162.9 mg, 0.75 mmol), the desired product was obtained as yellow crystals (19.1 mg, 30%), after purification by FC (SiO_2, Hexane/AcOEt 65:35) and crystallization from DCM/*n*-hexane. ^{1}H-NMR (300 MHz, $CDCl_3$) δ: 8.45 (d, *J* = 1.4 Hz, 1H); 8.23 (dd, *J* = 8.6, 1.77 Hz, 1H); 8.18 (d, *J* = 8.6 Hz, 1H); 7.31 (m, 4H); 4.20 (t, *J* = 7.1, Hz, 2H); 3.11 (t, *J* = 7.3 Hz, 2H). MS-APCI: Calc. for $C_{15}H_{12}N_2O_3S$: 300.1, Found: 301.1 $[M+H]^+$. LC-UV purity *t*R: 11.2 min – 99.8%. mp = 188-191 °C.

5-Methoxy-2-phenethylbenzo[*d*]isothiazol-3(2*H*)-one 26. Starting from compound **23c** (667.6 mg, 3.3 mmol), the desired product was obtained as brown crystals (499.7 mg, 55%), after purification by FC (SiO_2, Hexane/AcOEt 80:20) and crystallization from DCM/*n*-hexane. ^{1}H-NMR (300 MHz, $CDCl_3$) δ: 7.45 (d, *J* = 2.5 Hz, 1H); 7.35 (d, *J* = 8.8 Hz, 1H); 7.30-7.16 (m, 6H); 4.09 (t,

J = 7.3 Hz, , 2H); 3.84 (s, 3H); 3.03 (t, *J* = 7.7 Hz, 2H). MS-APCI: Calc. for $C_{16}H_{15}NO_2S$: 285.1, Found: 286.2 $[M+H]^+$. LC-UV purity: *t*R 13.30 min - 98.1%. mp = 75-77 °C.

6-Methoxy-2-phenethylbenzo[*d*]isothiazol-3(2*H*)-one 27. Starting from compound **23d** (1195.3 mg, 5.7 mmol), the desired product was obtained as brown crystals (677.6 mg, 42%), after purification by FC (SiO_2, Hexane/AcOEt 70:30) and crystallization from DCM/*n*-hexane 1:1. H-NMR (400 MHz, $CDCl_3$) δ: 7.93 (d, *J* = 8.6 Hz, 1H); 7.32-7.26 (m, 5H); 6.98-6-94 (m, 2H); 4.11 (t, *J* = 7.3 Hz, 1H); 3.90 (s, 3H); 3.07 (t, *J* = 7.3 Hz, 2H). MS-APCI: Calc. for $C_{16}H_{15}NO_2S$: 285.1, Found: 286.1 $[M+H]^+$. LC-UV purity: *t*R 9.1 min - 99.8%. mp = 82-85 °C.

7-Methyl-2-phenethylbenzo[*d*]isothiazol-3(2*H*)-one 28. Starting from compound **23e** (308.8 mg, 1.19 mmol), the desired product was obtained as a brown solid (40.1 mg, 19%), after purification by FC (SiO_2, Hexane/AcOEt 70:30, then Hexane/AcOEt 50:50). ^{1}H-NMR (300 MHz, $CDCl_3$) δ: 7.88 (dd, *J* = 7.1, 1.0 Hz, 1H); 7.37-7.22 (m, 8H); 4.15 (t, *J* = 7.5 Hz, 2H); 3.09 (t, *J* = 7,3 Hz, 2H); 2.34 (s, 3H). MS-ESI: Calc. for $C_{16}H_{15}NOS$: 269.1, Found: 270.2 $[M+H]^+$. LC-UV purity: *t*R 11.2 min - 97.8%. mp = 65-67 °C.

5-Hydroxy-2-phenethylbenzo[*d*]isothiazol-3(2*H*)-one 29. Compound **26** (99.1 mg, 0.35 mmol) was dissolved under nitrogen atmosphere in anhydrous benzene at 0 °C. BBr_3 (2.1 equiv) was added dropwise while the reaction turned deep brown. The mixture was warmed to rt and refluxed for 1 h. After being cooled to rt, the reaction was quenched with an aqueous saturated solution of $NaHCO_3$. The mixture was diluted with AcOEt, the organic layer was washed with water and brine. The organic phases were collected, dried over Na_2SO_4 and the solvent was removed under reduced pressure. After purification by FC (SiO_2, Hexane/AcOEt 50:50) and crystallization from EtOH/H_2O 1:1, **29** (33.2 mg, 35%) was obtained as a light yellow powder. ^{1}H-NMR (300 MHz, $CDCl_3$) δ: 7.70 (d, *J* = 2.4 Hz, 1H); 7.40 (d, *J* = 8.7, Hz, 1H); 7.28 (m, 6H); 4.14 (t, *J* = 7.4 Hz, 2H); 3.08 (t, *J* = 7.7

Hz, 2H). MS-APCI: Calc. for $C_{15}H_{13}NO_2S$: 271.1, Found: 272.3 $[M+H]^+$. LC-UV purity: *t*R 9.8 min – 98.5%. mp = 161-163 °C.

6-Hydroxy-2-phenethylbenzo[*d*]isothiazol-3(2*H*)-one 30. Compound **27** (200.0 mg, 0.70 mmol) was dissolved under nitrogen atmosphere in anhydrous benzene at 0 °C. BBr_3 (2.1 equiv) was added dropwise while the reaction turned deep brown. The mixture was warmed to rt and refluxed for 1 h. After being cooled to rt, the reaction was quenched with an aqueous saturated solution of $NaHCO_3$. The mixture was diluted with AcOEt, the organic layer was washed with water and brine. The organic phases were collected, dried over Na_2SO_4 and the solvent was removed under reduced pressure. After purification by FC (SiO_2, Hexane/AcOEt 50:50) and crystallization from EtOH/H_2O 1:1, final product **30** (46.9 mg, 25%) was obtained as a light yellow powder. ^{1}H-NMR (300 MHz, CD_3OD) δ: 7.74 (d, *J* = 8.6 Hz, 1H); 7.26-7.18 (m, 5H); 7.02 (d, *J* = 2.0 Hz, 1H); 6.87 (dd, *J* = 8.6, 2.0 Hz, 1H); 4.07 (t, *J* = 7.4 Hz, 2H); 3.03 (t, *J* = 7.7 Hz, 2H). MS-APCI: Calc. for $C_{15}H_{13}NO_2S$: 271.1, Found: 272.3 $[M+H]^+$. LC-UV purity: *t*R 7.0 min - 99.3%. mp = 172 °C.

***Tert*-butyl (3-oxobenzo[*d*]isothiazol-2(3*H*)-yl)carbamate 31**. The title compound was prepared with a modification with respect to the originally reported procedure.[49] To a stirred solution of *N*-Boc hydrazine (817.8 mg, 6.19 mmol) and anhydrous TEA (2.75 mL, 19.7 mmol) in THF (8.0 mL) at 0 °C, a solution of 2,2'-dithiobisbenzoyl chloride,[69] (1129.1 mg, 3.29 mmol) in THF (7.0 mL) was added dropwise with stirring. The reaction was allowed to warm to rt over the course of 16 h, after when a solution of I_2 (1838.7 mg, 7.24 mmol) in THF (10.0 mL) was added dropwise. The mixture was stirred for 4 h, diluted with AcOEt and the organic layer washed sequentially with an aqueous phosphate buffer solution, aqueous diluted $Na_2S_2O_3$, water and brine. The organic layer was dried over Na_2SO_4 and filtered. The solvents were removed under reduced pressure and the residue was purified by column chromatography (SiO_2, Hexane/AcOEt 70:30) to afford **31** (874.1 mg, 53%) as a white amorphous solid. Analytical data agree with those reported.[70]

General method G. To a cold (0 °C) solution of **31** in anhydrous DMF, KHMDS (1.2 equiv) was added in small portions. The reaction was stirred under nitrogen atmosphere for 10 min, when a solution of the alkyl halide in anhydrous DMF was added. The solution was gradually warmed to tr and stirred for 16 h. The solvent was removed under reduced pressure and the residue was partitioned between AcOEt and an aqueous phosphate buffer solution. The aqueous layer was extracted 3 times with AcOEt. The organic layer was dried over Na_2SO_4, filtered and the solvent evaporated under reduced pressure affording the crude product that was subjected to flash column chromatography.

***Tert*-butyl benzyl(3-oxobenzo[*d*]isothiazol-2(3*H*)-yl)carbamate 32a**. Starting from compound **31** (700.0 mg, 2.62 mmol) and benzyl bromide (380 μL, 3.15 mmol), **32a** (586.2 mg, 62%) was obtained as a white solid after purification by FC (SiO_2, Hexane/AcOEt 80:20). ^{1}H-NMR (300 MHz, $CDCl_3$) δ: 8.04 (d, *J* = 8.5 Hz, 1H); 7.57 (d, *J* = 8.3 Hz, 1H); 7.27 (m, 7H); 5.28 (d, *J* = 14.7 Hz, 1H); 4.49 (d, *J* = 14.8 Hz, 1H); 1.41 (bs, 9H).

Methyl 4-(((*tert*-butoxycarbonyl)(3-oxobenzo[*d*]isothiazol-2(3*H*)-yl)amino)methyl)benzoate 32b. Starting from compound **31** (213.0 mg, 0.80 mmol) and methyl 4-(bromomethyl)benzoate after purification by FC (SiO_2, Hexane/AcOEt 80:20), **32b** (237.1 mg, 71%) was obtained as a yellow oil. ^{1}H-NMR (400 MHz, $CDCl_3$) δ: 8.01 (m, 3H), 7.58 (t, *J* = 7.2 Hz, 1H); 7.43 (d, *J* = 8.0 Hz, 2H); 7.34 (m, 2H); 5.25 (bd, *J* = 17.5 Hz, 1H); 4.56 (bd, *J* = 15.0 Hz, 1H); 3.89 (s, 3H); 1.41 (bs, 9H).

***Tert*-butyl 4-(((*tert*-butoxycarbonyl)(3-oxobenzo[*d*]isothiazol-2(3*H*)-yl)amino)methyl)benzoate 32c**. Starting from compound **31** (163.3 mg, 0.61 mmol) and *tert*-butyl 4-(bromomethyl)benzoate after purification by FC (SiO_2, Hexane/AcOEt 90:10), **32c** (150.2 mg, 57%) was obtained as a

yellow oil. ^{1}H-NMR (300 MHz, $CDCl_3$) δ: 8.01 (d, *J* = 7.8 Hz, 1H); 8.94 (d, *J* = 8.2 Hz, 2H); 7.57 (t, *J* = 7.3 Hz, 1H); 7.41-7.31 (m, 4H); 5.25 (bd, *J* = 14.0 Hz, 1H); 4.55 (bd, *J* = 15.0 Hz, 1H); 1.56 (s, 9H); 1.40 (bs, 9H).

***Tert*-butyl ([1,1'-biphenyl]-4-ylmethyl)(3-oxobenzo[*d*]isothiazol-2(3*H*)-yl)carbamate 32d**. Starting from compound **31** (178.8 mg, 0.67 mmol) and 4-(bromomethyl)-1,1'-biphenyl after purification by FC (SiO_2, Hexane/AcOEt 90:10), product **32d** (220.7 mg, 76%) was obtained as a white solid. ^{1}H-NMR (300 MHz, $CDCl_3$) δ: 8.04 (d, *J* = 7.4, 1H); 7.60-7.55 (m, 5H); 7.45-7.25 (m, 7H); 5.30 (bd, *J* = 16.1 Hz, 1H); 4.53 (bd, *J* = 14.9, 1H); 1.45 (bs, 9H).

2-(Benzylamino)benzo[*d*]isothiazol-3(2*H*)-one 33. Starting from intermediate **32a** (403.1 mg, 1.12 mmol) after purification by FC (SiO_2, DCM/AcOEt 97:3) and crystallization from *n*-hexane final product **33** (202.9 mg, 70%) was obtained as white crystals. ^{1}H-NMR (300 MHz, DMSO-d_6) δ: 7.83 (t, *J* = 8.5 Hz, 2H); 7.64 (t, *J* = 7.2 Hz, 1H); 7.32 (m, 6H); 6.76 (t, *J* = 4.1 Hz, 1H); 4.19 (d, *J* = 4.0 Hz, 2H). MS-APCI: Calc. for $C_{14}H_{12}N_2OS$: 256.1, Found: 257.2 $[M+H]^+$. LC-UV purity: *t*R 8.98 min – 97.6%. mp = 110 °C.

Methyl 4-(((3-oxobenzo[*d*]isothiazol-2(3*H*)-yl)amino)methyl)benzoate 34. Starting from intermediate **32b** (237 mg, 0.57 mmol) after purification by FC (SiO_2, Hexane/AcOEt 70:30) and crystallization from DCM/hexane final product **34** (90 mg, 50%) was obtained as white crystals. ^{1}H-NMR (300 MHz, $CDCl_3$) δ: 8.00 (m, 3H); 7.60 (t, *J* = 7.3 Hz, 1H); 7.50 (d, *J* = 8.2 Hz, 2H); 7.38 (m, 2H); 5.41 (bs, 1H); 4.36 (s, 1H); 3.90 (s, 3H). MS-ESI: Calc. for $C_{16}H_{14}N_2O_3S$: 314.1, Found: 315.2 $[M+H]^+$. LC-UV purity: *t*R 6.6 min – 98.9%. mp = 174 – 176 °C.

4-(((3-Oxobenzo[*d*]isothiazol-2(3*H*)-yl)amino)methyl)benzoic acid 35. Starting from intermediate **32c** (150 mg, 0.3 mmol) after purification by FC (SiO_2, Hexane/AcOEt 40:60) final

product **35** (60 mg, 61%) was obtained as a white powder. ^{1}H-NMR (300 MHz, CD_3COOD) δ: 8.04 (d, *J* = 8.2 Hz, 3H); 7.61 (m, 4H); 7.44 (dt, *J* = 8.0, 1.8 Hz, 1H); 4.40 (s, 2H). MS-ESI: Calc. for $C_{15}H_{12}N_2O_3S$: 300.1, Found: 301.3 $[M+H]^+$. LC-UV purity: *t*R 7.1 min – 96.3%. mp = 215 °C (dec.).

2-(([1,1'-Biphenyl]-4-ylmethyl)amino)benzo[*d*]isothiazol-3(2*H*)-one 36. Starting from intermediate **32d** (220.3 mg, 0.51 mmol) after purification by FC (SiO_2, Hexane/AcOEt 70:30) final product **36** (101.5 mg, 60%) was obtained as a white powder. ^{1}H-NMR (300 MHz, $CDCl_3$) δ: 8.03 (d, *J* = 7.9 Hz, 1H); 7.60-7.33 (m, 12H); 5.02 (bs, 1H); 4.35 (s, 2H). MS-APCI: Calc. for $C_{20}H_{16}N_2OS$: 332.1, Found: 333.3 $[M+H]^+$. LC-UV purity: *t*R 14.9 min – 96.0%. mp = 148-151 °C.

2-(Benzyl(methyl)amino)benzo[*d*]isothiazol-3(2*H*)-one 37: To a solution of 2-(benzylamino)benzo[*d*]isothiazol-3(2H)-one **33** (58.8 mg, 0.23 mmol) in MeI (0.7 mL, 11.18 mmol), imidazole (16.0 mg, 0.24 mmol) was added in one portion. The reaction was stirred at rt for 16 h. The solvent was evaporated under reduced pressure and the residue was directly purified by FC (SiO_2, DCM/MeOH 99:1) affording **37** (39 mg, 64%) of product as a pale yellow waxy solid. ^{1}H-NMR (300 MHz, $CDCl_3$) δ: 8.00 (d, *J* = 7.9 Hz, 1H); 7.58 (td, *J* = 8.0, 1.2 Hz, 1H); 7.44 (d, *J* = 8.0 Hz, 1H); 7.25-7.35 (m, 4H); 4.24 (s, 2H); 2.95 (s, 3H). MS-APCI: Calc. for $C_{15}H_{14}N_2OS$: 270.1, Found: 271.3 $[M+H]^+$. LC-UV purity: *t*R 9.6 min – 95.6%. mp = 142 °C.

Di-*tert*-butyl pentane-1,5-diylbis((3-oxobenzo[*d*]isothiazol-2(3*H*)-yl)carbamate) 38a. Starting from compound **31** (497.9 mg, 1.87 mmol) and 1,5-diiodopentane (170 μL, 1.1 mmol) after purification by FC (SiO_2, Hexane/AcOEt 70:30), **38a** (294.3 mg, 45%) was obtained as a light yellow solid. ^{1}H-NMR (400 MHz, $CDCl_3$) δ: 8.00 (d, *J* = 7.8 Hz, 2H); 7.60 (t, *J* = 7.6 Hz, 2H); 7.44 (d, *J* = 8.1 Hz, 2H); 7.34 (t, *J* = 7.5 Hz, 2H); 3.75-3.60 (m, 4H); 1.69-1.35 (m, 24H).

Di-*tert*-butyl hexane-1,5-diylbis((3-oxobenzo[*d*]isothiazol-2(3*H*)-yl)carbamate) 38b. Starting from compound **31** (496.8 mg, 1.86 mmol) and 1,6-diiodohexane (170 μL, 1.1 mmol) after purification by FC (SiO_2, Hexane/AcOEt 80:20), **38b** (303.7 mg, 57%) was obtained as a white foam. ^{1}H-NMR (400 MHz, $CDCl_3$) δ: 8.00 (d, *J* = 7.8 Hz, 2H); 7.60 (t, *J* = 7.3 Hz, 2H); 7.44 (d, *J* = 8.1 Hz, 2H); 7.34 (t, *J* = 7.6 Hz, 2H); 3.72 (q, *J* = 7.4 Hz, 2H); 3.57 (q, *J* = 7.4 Hz, 2H); 1.66-1.36 (m, 26H).

General method H. To a solution of precursor **32a-d**, **38a-b** in DCM (5.0 mL), TFA (5.0 mL) was added dropwise at 0 °C. The reaction was gently warmed to rt and stirred for 4 h. The volatiles were removed under reduced pressure and the residue was dissolved in AcOEt and washed twice with an aqueous saturated solution of $NaHCO_3$ and once with brine. The organic phase was dried over Na_2SO_4, filtered and the solvent evaporated under reduced pressure affording the crude product that was subjected to flash column chromatography.

2,2'-(Pentane-1,5-diylbis(azanediyl))bis(benzo[*d*]isothiazol-3(2*H*)-one) 39. Starting from intermediate **38a** (294 mg, 0.5 mmol) after purification by FC (SiO_2, Hexane/AcOEt 30:70) final product **24** (146 mg, 75%) was obtained as a white solid. ^{1}H-NMR (300 MHz, $CDCl_3$) δ: 8.00 (d, *J* = 7.8 Hz, 2H); 7.60 (t, *J* = 7.6 Hz, 2H); 7.47 (d, *J* = 8.0 Hz, 1H); 7.37 (t, *J* = 7.5 Hz, 2H); 4.58 (bs, 2H); 3.15 (t, *J* = 6.6 Hz, 4H); 1.64-1.48 (m, 6H). MS-ESI: Calc. for $C_{19}H_{20}N_4O_2S_2$: 400.1, Found: 401.5 $[M+H]^+$. LC-UV purity: *t*R 7.9 min - 98.4%. mp = 128-131 °C.

2,2'-(Hexane-1,5-diylbis(azanediyl))bis(benzo[*d*]isothiazol-3(2*H*)-one) 40: Starting from intermediate **38b** (327.4 mg, 0.53 mmol) after purification by FC (SiO_2, Hexane/AcOEt 20:80) final product **40** (106.0 mg, 48%) was obtained as a white solid. ^{1}H-NMR (400 MHz, $CDCl_3$) δ: 8.03 (d, *J* = 7.9 Hz, 2H); 7.62 (t, *J* = 7.6 Hz, 2H); 7.51 (d, *J* = 8.0 Hz, 2H); 7.40 (t, *J* = 7.5 Hz, 2H); 4.15 (bs,

2H); 3.17 (t, *J* = 6.6 Hz, 2H); 1.62-1.44 (m, 8H). MS-ESI: Calc. for $C_{20}H_{22}N_4O_2S_2$: 414.1, Found: 415.4 $[M+H]^+$. LC-UV purity: *t*R 9.4 min - 99.0%. mp = 151-154 °C.

MGL Enzyme Assay. In vitro MGL activity was measured as previously described.[22,71] Briefly, we transiently transfected HeLa cells with plasmid DNA encoding recombinant rat MGL in the pEF6/V5-His, using the Superfect reagent (Qiagen). After harvesting cells in ice-cold 50 mM Tris-HCl, pH 8.0, containing 0.32 M sucrose, cell homogenates were prepared by sonicating the cells for 1 min on ice, followed by three cycles of freeze-thaw. Protein concentration was determined using Pierce Bicinchoninic acid (BCA) protein assay kit (Thermo Fisher Scientific). For the in vitro activity assay, homogenates were pre-incubated with the indicated concentration of testing drugs for 10 min at 37 °C in the assay buffer (50 mM Tris-HCl, pH 8.0, containing 0.5 mg/mL fatty acid-free BSA). The enzyme substrate 2-oleoylglycerol (2-OG), which we use in preference to 2-AG to increase the signal-to-noise ratio in the assay, was added to the mixture to the final concentration of 10 μM, and incubated for additional 10 min at 37 °C. Reactions were stopped by adding chloroform/methanol (2:1, vol/vol), containing heptadecanoic acid (5 nmol/sample) as an internal standard. After centrifugation at 2,000 x g at 4 °C for 10 min, the bottom organic layers were collected, and dried under N_2 stream. The lipid extracts were suspended in chloroform/methanol (1:3, vol/vol) and analyzed by an LC-MS method as described.[71]

Site-Directed Mutagenesis. Site-directed mutagenesis was made using a QuikChange II XL Kit (Strategene) following manufacturer's instructions. We used rat MGL-pEF6/V5-His plasmid DNA as a template[41] and verified all plasmids by DNA sequencing.

Rapid Dilution Assay. Rapid dilution assays were performed as previously described[72] using purified MGL that was prepared as previously described.[22] Briefly, samples containing purified MGL (100-fold concentrated compared with standard assays) were preincubated with 10-fold the

IC_{50}-equivalent concentration of the compound 13, MAFP or vehicle (dimethylsulphoxide, DMSO, final concentration 2%) for 20 min at 37 °C. Reactions were then diluted 100-fold with assay buffer containing substrate 2-OG to initiate reactions, and the time course of product (oleic acid) formation was measured by LC-MS.

In vivo properties of compound 13. All procedures met the National Institutes of Health guidelines for the care and use of laboratory animals and were approved by the Institutional Animal Care and Use Committee of the University of California, Irvine. Adult male C57/BL6 mice (n=4 for each group) received either **13** (10 mg/kg) or vehicle (saline) by i.p. injection. At the indicated time points after the injection, the animals were euthanized and plasma and brains were collected for analysis.

Compound **13** was quantified using a LC-MS/MS method developed in our laboratory. Briefly, brains were homogenized in 5 mL of acetonitrile containing 0.1% formic acid and soluble fractions were passed through Captiva EMR-Lipid cartridges (EMR) (Agilent Technologies, Wilmington, DE). The cartridges were eluted with water:acetonitrile (1:4, v/v), the samples were evaporated under nitrogen, and reconstituted in methanol (100 µL) for LC/MS analysis. For plasma samples, plasma (100 µL) was diluted with acetonitrile containing 0.1% formic acid (0.5 mL) and subjected to EMR fractionation, as described above. A Zorbax Eclipse XDB C18, 1.8 µm, 2.1 x 30 mm column was used for LC/MS analysis of compound **13**. The mobile phase consisted of - A: 0.1 % formic acid in water, B: 0.1 % formic acid in methanol. A step gradient was utilized, with 55 % B for 1.5 min followed by 95 % B for 2.0 min. Flow rate was 0.5 mL/min and injection volume was 5.0 µL. Column temperature was maintained at 40 °C. A 6460C triple quadruple mass spectrometric detector (MSD) with Agilent Jet Stream source interface (Agilent Technologies, Santa Clara, CA) was used. The MSD source parameters were as follows: drying gas flow was 10 L/min at 300 °C, and sheath gas flow was 10 L/min at 300 °C. Nebulizer pressure was 40 psi. Capillary and nozzle voltages were maintained at 3,500 V and 500 V, respectively. MS acquisition

parameters, under positive mode ESI, obtained by Agilent MassHunter Optimizer software, were precursor *m/z* = 256.1 and product *m/z* = 105.0, with collision energy at 17 V and fragmentation energy 109 V. Limit of detection (signal/noise > 3.0) was 0.05 ng/mL and limit of quantification (signal/noise > 10) was 0.1 ng/mL. Linear calibration range was 0.1 ng/mL to 100.0 ng/mL, with a $1/x^2$ weighted R^2 of > 0.98.

2-AG quantitation in the brain. Lipids were extracted from the brain homogenate, and the levels of 2-AG were determined by an LC-MS method as described previously with minor modification.[39] Briefly, we used an Agilent 1200 LC system coupled to a 6410 triple quadrupole MS system (Agilent Technologies, Palo Alto, CA). The column was a ZORBAX Eclipse XDB-C18 (4.6 × 50 mm, 1.8 μm, Agilent Technologies). We used an isocratic elution method as follows: 80 % solvent A consisted of methanol with 0.25% acetic acid and 5 mM ammonium acetate, and 20% solvent B consisted of water with 0.25% acetic acid and 5 mM ammonium acetate. Lipids were eluted at a flow rate of 0.5 mL/min. Column temperature was held at 40 °C. MS detection was in electrospray ionization (ESI) and positive ionization mode, with capillary voltage at 3.5 kV and fragmentor voltage at 135 V. N_2 was used as drying gas at a flow rate of 12 L/min and temperature of 350 °C. Nebulizer pressure was set at 50 psi. Quantifications were conducted by an isotope dilution method, monitoring $[M+H]^+$ in the selected ion monitoring (SIM) mode. The multiple reaction transitions monitored were as follows: 2-AG, *m/z* 379 → 287; $^2H_5$-2-AG, *m/z* 384 → 292. Detection and analysis were performed using Mass Hunter Workstation software (Agilent).

Lactate dehydrogenase release in Neuro-2a cells. Cellular toxicity was determined by measuring the release of Lactate dehydrogenase (LDH) in the culture media, using a Cytotoxicity Detection Kit^{Plus} (Roche Diagnostics). Briefly, cells were seeded in 96-well plates at a concentration of 5×10^3 cells/well. After 24 h, they were treated with agents for 30 min, followed by a treatment with H_2O_2 (300 μM) for 24 h. Absorbance was measured using a SpectraMax M5 microplate reader (Molecular Devices).

Statistical Analyses. All results are expressed as mean ± SEM. Non-linear regression analyses were performed using Prism version 5.0 (GraphPad Software). Statistical significance was assessed by two-tailed Student's t test or one-way ANOVA with Dunnett's post test.

DGL Activity. DGL activity was measured as previously described.[73] Briefly, rat brains were homogenized in ice-cold 50 mm Tris-HCl, pH 7.0, and homogenates were centrifuged (800 × *g* for 5 min at 4 °C). DGL activity was measured using the supernatant (100 µg of protein) at 37 °C for 30 min in 50 mM Tris-HCl, pH 7.0, containing 0.1% Triton X-100, and the substrate diheptadecanoylglycerol (50 µM). Reactions were stopped by adding chloroform/methanol (1:1) containing [$^2H_5$]-2-AG. Lipids were extracted, and the levels of reaction product monoheptadecanoylglycerol $[M+Na]^+$ (*m/z* = 367) were quantified by LC/MS-MS using [$^2H_5$]2-AG (*m/z* = 406) as an internal standard.

FAAH Activity. FAAH activity was measured as previously described.[74] Briefly, rat brains were homogenized in ice-cold Tris buffer (50 mM, pH 7.5) containing sucrose (0.32 M). The homogenates were centrifuged at 1000 × *g* for 10 min at 4 °C, and activity was measured in the supernatant using [^{3}H]anandamide (anandamide[ethanolamine-^{3}H], 60 Ci mmol^{-1}, American Radiolabeled Chemicals, St. Louis, USA) as substrate. Homogenates (50 µg protein) were incubated for 30 min at 37 °C in Tris buffer (50 mM, pH 7.5, 0.5 mL) containing fatty-acid-free bovine serum albumin (BSA, 0.05%, w/v), 10 µM anandamide, and [^{3}H]anandamide (20,000 cpm), and varying concentrations of test compounds. The drugs were dissolved in DMSO and final DMSO concentration was 1%. The reactions were stopped by adding 1 mL of $CHCl_3$/MeOH (1:1) and centrifugation at 2000 × *g* for 10 min at 4 °C. Radioactivity in the aqueous layer ([^{3}H]ethanolamine) was measured by liquid scintillation counting.

ABHD6 Activity. Homogenates of HEK293 cells stably expressing mouse ABHD6 were used to measure activity with 2-AG as substrate, and measuring glycerol production as described in ref. 75.

CB_1 and CB_2 binding assays. The binding affinity of compound **13** for rat CB_1 and CR_2 receptors was evaluated through Euroscreen Fast[76] assays FAST-044B and FAST-045B, using receptors expressed in CHO-K1 cell lines and [^{3}H]-SR141716A and [^{3}H]-CP55,940 as radioligand, respectively. Compound **13** was tested at 50, 500 and 1000 nM concentrations in technical duplicates.

TRPA1 and TRPV1 agonist and antagonist assays. Compound **13** was evaluated as agonist and antagonist of human TRPA1 and TRPV1 ion channels through Euroscreen Fast[76] aequorin-based calcium mobilization assays FAST-1301A and FAST1300A, respectively. Tests were performed in CHO-K1-mt aequorin cell line, using allyl isothiocyanate and resiniferatoxin as reference agonists and A 967079 and capsazepine as reference antagonists for TRPA1 and TRPV1, respectively. Compound **13** was tested at fixed 50, 500 and 1000 nM concentrations in the antagonist assay and at the concentrations of 100, 1000 and 2000 nM in the agonist assay, in in technical duplicates.

Computational studies. Molecular modeling studies were performed using the Schrödinger software suite. BTZ derivatives were built in Maestro 9.2[77] and prepared with Ligprep 2.5;[78] the protein structure was refined using the Protein Preparation Wizard tool.[79] Covalent docking was performed with Prime 3.0,[80,81,82] and noncovalent docking with Glide 5.7.[83,84]

***Protein preparation*.** The crystal structure of human MGL (PDB 3HJU, chain A),[85] in which the lid domain is in an open conformation, was used as model structure for docking studies. Hydrogen atoms were added, and the hydrogen bonding network was optimized by sampling the conformation of histidine, asparagine and glutamine side chains; the orientation of thiol and hydroxyl groups was also optimized. Basic and acidic residues were modeled in their positively and negatively charged

form, respectively, while histidine residues were maintained in their neutral form. The resulting structure was subjected to a restrained minimization with the OPLS2005 force field[86] in which only hydrogen atoms were free to move. A second minimization was performed by restraining the heavy atoms to an RMSD value of 0.3 Å.

Covalent docking studies. The Prime Covalent Docking tool was used to perform covalent docking studies. To allow ligand accommodation, the attachment residue (Cys201) and residues within 8 Å from Cys201 were allowed to adjust in the loop sampling procedure. Ligands were prepared using Ligprep 2.5 and then minimized with Macromodel 9.9,[87] applying the OPLS2005 force field to an energy gradient of 0.05 kJ mol^{-1} $Å^{-1}$. Twenty poses were generated for each compound and ranked according to the Prime Energy values. The top ranked poses were selected and subjected to energy minimization to an energy gradient of 0.05 kJ mol^{-1} $Å^{-1}$. During energy minimization, the ligands and residues within 8 Å from them were free to move, while the backbone atoms of the other residues were kept fixed. The minimized pose characterized by best Prime Energy value for compounds **13** and **33** is represented in Figure 6.

Docking studies. Docking studies were performed to evaluate the binding mode of compounds **39** and **40**. The Induced Fit Docking (IFD) protocol was applied to account for both ligand and protein flexibility during the ligand docking procedure. As a first step, a softened-potential docking was performed by applying van der Waals radii scaling factors of 0.6 and 0.5 on the non-polar atoms of the protein and the ligands, respectively. Energy grids for the first docking runs were centered on Cys201 and Cys208. The enclosing box dimensions were set to 10×10×16 Å, to include the entire region spanning from Cys201 to Cys208, while the bounding box dimensions were set to 30×30×36 Å. Inhibitors **39** and **40**, which were previously prepared with Ligprep 2.5, were flexibly docked in the standard precision mode with default settings, and the five poses with best Glide score were retained for each ligand. The resulting complexes were then subjected to a protein refinement step. In this stage, residues within a distance of 6 Å from the ligand pose were refined through a side-chain conformational search and finally energy-minimized through the Prime

minimization. In the final step of the IFD procedure the ligand structures were optimized in the field of the refined receptor binding site, by applying the *mininplace* option. The complexes were evaluated according to their IFD score and the best one for each ligand was energy-minimized with Macromodel 9.9, applying the OPLS2005 force field to an energy gradient of 0.05 kJ mol^{-1} $Å^{-1}$. The complex obtained for compound 39 is depicted in Figure 7.

Free energy studies. The computational protocol described in ref. 40 was applied to this study. Human MGL modelled with a molecule of compound **13** covalently bound to Cys201 (Figure 5A) was embedded in a POPC lipid bilayer model according to the coordinates of the 3HJU crystal structure deposited into the Orientation of Protein in Membrane (OPM)[88] database, and the protein-membrane system was then solvated with approximatively 63000 spc water molecules in a simulation box of 84×81×136 Å. The OPLS2005 force field implemented in Desmond 3.6[89] was used to model the system. Bond lengths to hydrogen atoms were constrained by applying the M-SHAKE algorithm. Short-range electrostatic interactions were cut off at 9 Å, whereas long-range electrostatic interactions were treated using the Smooth Particle Mesh Ewald method.[90] A RESPA integrator was used with a time-step of 2 fs, while long-range electrostatic interactions were computed every 6 fs. The system was relaxed using a modified version of a relaxation protocol implemented in the Desmond package. The protocol consisted of a membrane relaxation step (a prolonged version of the membrane relaxation protocol provided by Desmond 3.6 implemented in the Schrodinger 2013-3 suite), with restrained protein. Membrane relaxation was then followed by a prolonged version of the system equilibration protocol provided by Desmond 3.6 (see Supporting Information for a detailed description of the relaxation protocol). The free energy profile of hMGL-**13** complex was computed using the well-tempered (wt) metadynamics implemented in Desmond 3.6. Distances between centers of mass of Cα of lid domain residues were used as CV1 (distance between 176-179 Cα and 150-157 Cα centers of mass) and as CV2 (distance between 176-179 Cα and 158-164 Cα centers of mass). The Gaussian width was set to 0.05 Å, the Gaussian height to

0.03 kcal/mol, and the interval between consecutive depositions was 0.09 ps. In wt metadynamics, Gaussians heights are resized taking into account the value of *V(s, t)*:

$$w_j = w \times exp\left(\frac{V_{(s,t_j}}{k_B \Delta T}\right)$$

where the initial height of the Gaussians w was 0.03 kcal/mol, kB is the Boltzmann constant and the sampling temperature ΔT was 1200 K. The wt metadynamics simulation lasted for 100 ns and was replicated. In order to evaluate the convergence of wt metadynamics simulations, we considered three criteria: 1) analysis of free energy surfaces (FESs) updated at intervals of 5 ns. We considered a simulation to be converged when the free energy profiles did not change significantly (Figure S7). 2) We checked that each collective variable had been completely explored with at least one recrossing, to avoid stopping the simulation with the system trapped in a specific free energy minimum (Figure S8). The evolution of the height of the Gaussians deposited throughout the wt metadynamics simulation was also registered (Figure S8). The sequence of damping and increasing phases indicates that depositions explored different minima several times. 3) We compared the FESs obtained from the two independent simulations and checked that, at convergence, they were superimposable (Figure S9).

High resolution mass spectrometry (HR-MS) characterization of human MGL-BTZ 13 complex.

Recombinant human MGL (Catalog Number: 7930-MG; Accession Number: Q99685) was supplied by R&D Systems (Minneapolis, MN, USA) as a 0.41 μg/μL 0.2 μm filtered stock solution in 25 mM Tris buffer pH 8.0 containing 1 M NaCl, 1 mM EDTA, 0.02 % v/v Brij35. It was an *E. coli* expressed protein with an N-terminal Met and a six His-tag. For the characterization of the intact MGL, 30 pmol of protein were incubated for 45 min at rt in 20 mM TRIS buffer, pH 8.0 (final incubation volume: 50 μL) either in the absence or in the presence of a 4:1 molar excess of compound **13**. At the end of the incubation time, intact protein samples were injected in a rapid desalting system constituted of a Waters Acquity HPLC (Waters Corp., Milford, MA, USA) with an

injection loop containing a Valco a 6-port injection valve[91] (VICI AG International, Schenkon, Switzerland) equipped with a micro-column[92] (approximately 2-μL bed volume of C4 Poros 20 R2) and proteins were eluted into an electrospray ion source at a flow rate of 40 μL/min employing a 8.5-min gradient going from 10 to 90 % acetonitrile in 0.1 % formic acid. Positive ion-electrospray ionization mass spectra of eluted proteins were acquired on a Waters Synapt G2 HDMS mass spectrometer (Waters Corp., Milford, MA, USA). A refrigerated Waters nano Acquity UPLC system for online pepsin digestion and rapid desalting of the protein samples was employed for peptide mass fingerprint analysis. The samples were passed through an online in-house packed digestion column (internal volume, 60 μL; IDEX, Oak Harbor, WA) packed with pepsin immobilized on agarose (Thermo Scientific, USA), at 200 μL/min solvent (0.23% formic acid, pH 2.3), and the peptides were trapped and desalted for 3 min.[93] The digestion protocol was carried out in the absence of the reducing agent Tris(2-carboxyethyl)phosphine (TCEP) to avoid the reductive cleavage of MGL-13 adduct. Peptides were eluted from the trap to the analytical column (Waters BEH C18, 1.7 μm, 1.0 mm × 100 mm) and separated with an 8−40 % gradient of 0.23% formic acid in acetonitrile (pH 2.3) over 7 min at a flow rate of 40 μL/min. To identify pepsin-generated peptides, mass spectral data were acquired on a Synapt HDMS system equipped with an ESI source and operated in the MS^E mode. The MS^E dataset was processed with ProteinLynx Global Server 3.0 (Waters Corp., Milford, MA, USA)[94] for searching against an "in house" protein database to which the recombinant human MGL sequence had been previously added.

Reactivity with glutathione. Stock solutions of all reagents were purged with argon and all reactions took place under argon atmosphere removing aliquots for analysis by syringe under positive argon pressure to minimize the potential interference of atmospheric oxygen. Reactions were initiated by injection of a 10 mM DMSO stock solution of BTZ **13** (final concentration: 100 μM) into a temperature equilibrated (37.0 °C) vial containing a buffered reaction solution with a 2-fold molar excess of glutathione (GSH) over benzisothiazolinone (final GSH concentration: 200

μM). Final concentration of DMSO was 1% v/v in 10 mM phosphate buffered saline (PBS) pH 7.4. In the aqueous medium in the presence of GSH, the existence of various equilibria could be appreciated. A steady-state condition was reached and at t=60 and t=120 min the concentrations of reactants and products were maintained. t=60 min was therefore chosen as the appropriate reaction time to investigate the identity and concentration of species in solution by LC/MS analysis. Disappearance of reacting BTZ **13** and formation of products was monitored by LC/UV using a gradient elution. Column used was a Supelco Discovery C_{18} column 150x4.6 mm i.d., 5 μm particle size (Supelco, Bellefonte, PA, USA). Eluent A: water additioned of 0.05% v/v trifluoroacetic acid (TFA); eluent B: methanol additioned of 0.05 % v/v TFA. Gradient was as follows: t(0 min): 95% A:5% B; t(6 min): 95% A:5% B; t(26 min): 5% A:95% B; t(28 min): 5% A:95% B returning to initial conditions in 0.5 min. Total gradient time was 30 min. Absorbance was monitored at the two wavelengths of 210 and 254 nm. Flow rate was 1 mL/min. Injected volume: 10 μL.

A Shimadzu HPLC gradient system (Shimadzu Corp., Kyoto, Japan) fitted with two LC-10AD Shimadzu pumps and a Shimadzu SPD-10 variable wavelength detector was employed for analysis. Standard curves for quantification of GSH and oxidized glutathione (GSSG) were prepared in PBS buffer and showed good linearity in the 5-500 μM concentration range. The limit of quantification (LOQ) was 5 μM, monitoring absorbance at λ = 210 nm. Standard curves for quantification of concentrations of BTZ 13 were prepared by spiking PBS buffer with stock solution of test compound in the 100 nM-100 μM concentration range. The limit of quantification (LOQ) was 100 nM, monitoring absorbance at λ = 254 nm. The coefficients of correlation (R^2) were > 0.99 for all curves.

Identity of reaction species was confirmed by LC/HR-MS analysis. Column used was a Phenomenex Sinergy Fusion (100x2.0mm i.d., 4 μm particle size (Phenomenex, Bologna, Italy). Eluent A: water additioned of 0.1 % v/v formic acid; eluent B: methanol additioned of 0.1 % v/v formic acid. Chosen gradient was as follows: t(0 min): 95% A:5% B; t(6 min): 95% A:5% B; t(26

min): 5% A:95% B; t(28 min): 5% A:95% B returning to initial conditions in 0.5 min. Total gradient time was 35 min. Flow rate was 350 μL/min. Injected volume: 10 μL. A Dionex UHPLC gradient system coupled to a Thermo LTQ Orbitrap mass spectrometer with an electrospray ionization (H-ESI) ion source was used for compound detection and analysis. Mass spectrometric analyses were done in positive ion mode and in full scan mode in the 150-750 amu range. ESI interface parameters were set as follows: probe middle (D) position; capillary temperature 275 °C; spray voltage 3.5 kV. Nitrogen was used as nebulizing gas at the following pressure: sheath gas 30 psi; auxiliary gas 10 arbitrary units (a.u.). Argon was used as the collision gas at a pressure of approximately 1.5 mtorr (1 torr = 133.3 Pa). The software Xcalibur, version 1.3 (Thermo Italia, Milan, Italy) was employed for data acquisition and processing.

Supporting information

The Supporting Information is available free of charge on the ACS Publications website.

HR-MS characterization of human MGL covalent complex with compound **13**, details on metadynamics symulations, LC-UV purity of target compounds (PDF). Molecular formula strings data (CSV). MGL covalent complex with compounds **13** and **33** (PDB). MGL complex with compound **39** (PDB).

Corresponding Author Information

Silvia Rivara, PhD

Dipartimento di Scienze degli Alimenti e del Farmaco,

Università degli Studi di Parma, Parco Area delle Scienze 27/A, I-43124 Parma, Italy

Phone: +39 0521 905061

Email: silvia.rivara@unipr.it

Acknowledgement

We are grateful to the Centro Interdipartimentale Misure "Giuseppe Casnati" of the University of Parma for providing NMR instrumentation. This work was carried out using the HPC (High Performance Computing) computational facilities of the University of Parma, Italy; http://www.hpc.unipr.it. The work was partially supported by NIH grant DA 026430 (to NS) and DA0444118 (to DP), by the Italian Ministry for University and Research (MIUR, PRIN 2017, 20175SA5JJ project, to MM) and the University of Parma (Progetti di Ateneo FIL Quota Incentivante 2019, to SR).

Abbreviations used

2-OG, 2-oleoylglycerol; ABHD6, alpha/beta hydrolase domain containing 6; BTZ, benzisothiazolinone; CB_1, cannabinoid receptor 1; CB_2, cannabinoid receptor 2; DABCO, 1,4-diazabicyclo[2.2.2]octane; DCE, dichloroethane; DCM, dichloromethane; DGL-α, diglyceride lipase; DMF, dimethylformamide; DMSO, dimethylsulphoxyde; FAAH, fatty acid amide hydrolase; FC, flash chromatography; FES, free energy surface; GSH, glutathione; ITZ, isothiazolinone; KHMDS potassium bis(trimethylsilyl)amide; MGL, monoacylglycerol lipase; NAC, *N*-acetyl cysteine; *t*R, retention time; SAR, structure-activity relationship; TEA, triethylamine; THF, tetrahydrofuran; TFA, trifluoroacetic acid; TMS, tetramethylsilane; TRPA1, transient receptor potential cation channel subfamily A member 1; TRPV1, transient receptor potential cation channel subfamily V member 1; wt, well-tempered.

References

[1] Okazaki, T.; Sagawa, N.; Okita, J. R.; Bleasdale, J. E.; Macdonald, P. C.; Johnson, J. M. Diacylglycerol metabolism and arachidonic acid release in human fetal membranes and decidua vera. *J. Biol. Chem.* **1981**, *256,* 7316–7321.

[2] Gulayas, A. I.; Cravatt, B. F.; Bracey, M. H.; Dinh, T. P.; Piomelli, D.; Boscia, F.; Freund, T. F.; Segregation of two endocannabinoid-hydrolyzing enzymes into pre- and postsynaptic compartements in the rat hippocampus, cerebellum and amygdala. *Eur. J. Neurosci.* **2004**, *20*, 441–458.

[3] Tornqvist, H.; Belfrage P. Purification and some properties of a monoacylglycerol-hydrolyzing enzyme of rat adipose tissue. *J. Biol. Chem*. **1976**, *251*, 813–819.

[4] Majerus P. W. Arachidonate metabolism in vascular disorders. *J. Clin. Invest*. **1983**, *72*, 1521–1525.

[5] Saario, S. M.; Laitinen, J. T. Monoglyceride lipase as an enzyme hydrolizing 2-arachidonoylglycerol. *Chem. Biodivers.* **2007**, *4*, 1903–1013.

[6] Dinh, T. P.; Carpenter, D.; Leslie, F. M.; Freund, T. F.; Katona, I.; Sensi, S. L.; Kathuria, S.; Piomelli, D. Brain monoglyceride lipase partecipatic in endocannabinoid inactivation. *Proc. Natl. Acad. Sci. U.S.A.* **2002**, *99*, 10819-10824. Erratum in the following: *Proc. Natl. Acad. Sci. U.S.A.* **2002**, *99*, 13961.

[7] Dinh, T. P.; Kathuria, S.; Piomelli, D. RNA interference suggests a primary role for monoacylglycerol lipase in the degradation of the endocannabinoid 2-acylglycerol. *Mol. Pharmacol.* **2004**, *66*, 1260–1264.

[8] Sugiura, T.; Kondo, S.; Sukugawa, A.; Nakane, S.; Shinoda, A.; Itoh, K.; Yamashita, A.; Waku, K. 2-Archidonoyl-glicerol: a possible endogenous cannabinoid receptor ligand in brain. *Biochem. Biophys. Res. Comm.* **1995**, *215*, 89–97.

[9] Mechoulam, R.; Ben-Shabat, S.; Hanus, L.; Ligumsky, M.; Kaminski, N. E.; Schatz, A. R.; Gopher, A.; Almog, S.; Martin, B. R.; Compton, D. R.; Pertwee, R. G.; Griffin, G.; Bayewitch, M.; Barg, J.; Vogel, Z. Identification of an endogenous 2-monoglyceride, present in canine gut, that binds to cannabinoid receptors. *Biochem. Pharmacol.* **1995**, *50*, 83–90.

[10] Wilson, R. I.; Nicoll, R. A. Endogenous cannabinoids mediate retrogade signalling at hippocampal synapses. *Nature* **2001**, *410*, 441–458.

[11] Kinsey, S. G.; Long, J. Z.; O'Neal, S. T.; Abdullah, R. A.; Poklis, J. L.; Boger, D. L.; Cravatt, B. F.; Lichtman, A. H. Blockade of endocannabinoid-degrading enzymes attenuates neuropathic pain. *J. Pharmacol. Exp. Ther.* **2009**, *330,* 902–910.

[12] Hohmann, A. G.; Suplita, N. M.; Bolton, N. M.; Neeley, M. H.; Fegley, D.; Mangieri, R.; Krey, J. F.; Walker, J. M.; Holmes, P. V.; Crystal, J. D.; Duranti, A.; Tontini, A.; Mor, M.; Tarzia, G.; Piomelli, D. An endocannabinoid mechanism for stress-induced analgesia. *Nature*, **2005**, *435*, 1108–1112.

[13] Melis, M.; Pillola, G.; Bisogno, T.; Minassi, A.; Petrosino, S.; Perra S.; Muntoni A. L.; Lutz, B.; Gessa, G. L.: Marsicano, G.; Di, M.; Pistis, V. M. Protective activation of the endocannabinoid system during ischemia in dopamine neurons. *Neurobiol. Dis.* **2006**, *24*, 15–27.

[14] Chen, X.; Zhang, J.; Chen, C. Endocannabinoid 2-arachidonoylglycerol protects neurons against β-amyloid insults. *Neuroscience* **2011**, *178*, 159–168.

[15] Kinsey, S. G.; O'Neal, S. T.; Long, J. Z.; Cravatt, B. F.; Lichtman, A. H. Inhibition of endocannabinoid catabolic enzymes elicits anxiolytic-like effects in the marble burying assay. *Pharmacol. Biochem. Behav.* **2011**, *98*, 21–27.

[16] Gokoh, M.; Kishimoto, S.; Oka, S.; Mori, M.; Waku, K.; Ishima, Y.; Sugiura, T. 2-Arachidonoylglycerol, an endogenous cannabinoid receptor ligand, induces rapid actin polymerization in HL-60 cells differentiated into macrophage-like. *Biochem. J.* **2005**, *386*, 583–589.

[17] Oka, S.; Ikeda, S.; Kishimoto, S.; Gokoh, M.; Yamagimoto, S.; Waku, K.; Sugiura, T. 2-Arachidonoylglycerol, an endogenous cannabinoid receptor ligand, induces the migration of EoL-1 human eosinophilic leukemia cells and human peripheral blood eosinophils. *J. Leukoc. Biol*. **2004**, *76*, 1002–1009.

[18] Nithipatikom, K.; Endsley, M. P.; Isbell, M. A.; Wheelock, C. E.; Hammock, B. D.; Campbell, W. D. A new class of inhibitors of 2-arachidonoylglycerol hydrolysis and invasion of prostatecancercells. *Biochem. Biophys. Res. Comm.* **2005**, *332*, 1028–1033.

[19] Bifulco, M.; Laezza, C.; Pisanti, S.; Gazzerro, P. Cannabinoids and cancer: pros and cons of an antitumor strategy *Br. J. Pharmacol.* **2006**, *148*, 123–135.

[20] Hohmann, A. G.; Suplita, R. L.; Bolton, N. M.; Neely, M. H.; Fegley, D.; Mangieri, R.; Krey, J. F.; Walker, J. M.; Holmes, P. V.; Crystal, J. D.; Duranti, A.; Tontini, A.; Mor, M.; Tarzia, G.; Piomelli, D. An endocannabinoid mechanism for stress-induced analgesia. *Nature* **2005**, *435*, 1108–1112.

[21] Makara, J. K.; Mor, M.; Fegley, D.; Szabó, S. I.; Kathuria, S.; Astarita, G.; Duranti, A.; Tontini, A.; Tarzia, G.; Rivara, S.; Freund, T. F.; Piomelli, D. Selective inhibition of 2-AG hydrolysis enhances endocannabinoid signaling in hippocampus. *Nat. Neurosci*. **2005**, *8*, 1139–1141.

[22] King, A. R.; Duranti, A.; Tontini, A.; Rivara, S.; Rosengarth, A. Clapper J.R.; Astarita, G.; Geaga, J. A.; Luecke, H.; Mor, M.; Tarzia, G.; Piomelli, D. URB602 inhibits monoacylglycerol lipase and selectively blocks 2-arachidonoylglycerol degradation in intact brain slices. *Chem. Biol.* **2007**, *14*, 1357–1365.

[23] Long, J. Z.; Li, W.; Booker, L.; Burston, J. J.; Kinsey, S. G.; Scholosburg, J. E.; Pavon, F. J.; Serrano, A. M.; Selley, D. E.; Parson, L. H.; Lichtman, A. H.; Cravatt, B. F. Selective blockade of 2-arachidonoylglycerol hydrolysis produces cannabinoid behavioral effects. *Nat. Chem. Biol.* **2009**, *5*, 37–44.

[24] McAllister, L. A.; Butler, C. R.; Mente, S.; O'Neil, S. V.; Fonseca, K. R.; Piro, J. R.; Cianfrogna, J. A.; Foley, T. L.; Gilbert, A. M.; Harris, A. R.; Helal, C. J.; Johnson, D. S.; Montgomery, J. I.; Nason, D. M.; Noell, S.; Pandit, J.; Rogers, B. N.; Samad, T. A.; Shaffer, C. L., da Silva, R. G.; Uccello, D. P.; Webb, D.; Brodney, M. A. Discovery of trifluoromethyl glycol carbamates as potent and selective covalent monoacylglycerol lipase (MAGL) inhibitors for treatment of neuroinflammation. *J. Med. Chem.* **2018**, *61*, 3008–3026.

[25] Cisar, J. S.; Weber, O. D.; Clapper, J. R.; Blankman, J. L.; Henry, C. L.; Simon, G. M.; Alexander, J. P.; Jones, T. K.; Ezekowitz, R. A. B.; O'Neill, G. P:, Grice C. A. Identification of ABX-1431, a selective inhibitor of monoacylglycerol lipase and clinical candidate for treatment of neurological disorders. *J. Med. Chem*. **2018**, *61*, 9062–9084.

[26] Granchi, C.; Lapillo, M.; Glasmacher, S.; Bononi, G.; Licari, C.; Poli, G.; El Boustani, M.; Caligiuri, I.; Rizzolio, F.; Gertsch, J.; Macchia, M.; Minutolo, F.; Tuccinardi, T.; Chicca, A. Optimization of a benzoylpiperidine class identifies a highly potent and selective reversible monoacylglycerol lipase (MAGL) inhibitor. *J. Med. Chem*. **2019**, *62*, 1932–1958.

[27] Aida, J.; Fushimi, M.; Kusumoto, T.; Sugiyama, H.; Arimura, N.; Ikeda, S.; Sasak,i M.; Sogabe, S.; Aoyama, K.; Koike, T. Design, synthesis, and evaluation of piperazinyl pyrrolidin-2-ones as a novel series of reversible monoacylglycerol lipase inhibitors. *J. Med. Chem*. **2018**, *61*, 9205–9217.

[28] Ollis, D. L.; Cheah, E.; Cycler, M.; Dijkstra, B.; Frolow, F.; Franken, S. M. The α/β hydrolase fold. *Protein Eng.* **1992**, *5*, 197–211.

[29] Karlsson, M.; Contreras, J. A.; Hellman, U.; Tornqvist, H.; Holm, C. cDNA cloning, Tissue distribution and identification of the catalytic triad of monoglyceride lipase. Evolutionary relationship to esterases, lysophospholipases and haloperoxidases. *J. Biol. Chem.* **1997**, *272*, 27218–27223.

[30] Scalvini L.; Piomelli, D., Mor M. Monoglygeride lipase: structure and inhibitors. *Chem. Phys. Lipids* **2016**, *197*, 13–24.

[31] Laitinen, T.; Navia-Paldanius, D.; Rytilahti, R.; Marjamaa, J. J.; Kařízková, J.; Parkkari, T.; Pantsar, T.; Poso, A.; Laitinen, J. T.; Savinainen, J. R. Mutation of Cys242 of human monoacylglycerol lipase disrupts balanced hydrolysis of 1- and 2-monoacylglycerols and selectively impairs inhibitor potency. *Mol. Pharmacol*. **2014**, *85*, 510–519.

[32] Matuszak, N.; Muccioli, G. G.; Labar. G.; Lambert. D. M. Synthesis and in vitro evaluation of N-substituted maleimide derivatives as selective monoglyceride lipase inhibitors. *J. Med. Chem.* **2009**, *52*, 7410–7420.

[33] Zvonok, N.; Pandarinathan, L.; Williams, J.; Johnston, M.; Karageorgos, I., Janero, D. L.; Krishnan, S. C.; Makriyannis, A. Covalent inhibitors of human monoacylglycerol lipase: ligand-assisted characterization of the catalytic site by mass spectroscopy and mutational analysis. *Chem. Biol.* **2008**, *15*, 854–862.

[34] Saario S. M.; Salo, O. M. H.; Nevalainen, T.; Poso A.; Laitinen J. T.; Järvinen, T.; Niemi, R. Characterization of the sulfhydryl-sensitive site in the enzyme responsible for hydrolysis of 2-arachidonoylglycerol in rat cerebellar membranes. *Chem. Biol.* **2005**, *12*, 649–656.

[35] Labar, G.; Bauvois, C.; Muccioli, G. G.; Wouters, J.; Lambert, D. M. Disulfiram is an inhibitor of human purified monoacylglycerol lipase, the enzyme regulating 2-arachidonoylglycerol signaling. *ChemBioChem.* **2007**, *8*, 1293–1297.

[36] King, A. R.; Dotsey, E. Y.; Lodola, A.; Jung, K. M.; Ghomian, A.; Qiu, Y.; Fu, J.; Mor, M.; Piomelli, D. Discovery of potent and reversible monoacylglycerol lipase inhibitors. *Chem. Biol*. **2009**, *16*, 1045–1052.

[37] Patel, J. C.; Rice, M. E. Classification of H_2O_2 as a neuromodulator that regulates striatal dopamine release on a subsecond time scale. *ACS Chem. Neurosci*. **2012**, *3*, 991–1001.

[38] Rice M. E. H_2O_2: a dynamic neuromodulator. *Neuroscientist* **2011**, *17*, 389–406.

[39] Dotsey, E.Y.; Jung, K.M.; Basit, A.; Wei, D.; Daglian, J.; Vacondio, F.; Armirotti, A.; Mor, M.; Piomelli, D. Peroxide-dependent MGL sulfenylation regulates 2-AG-mediated endocannabinoid signaling in brain neurons. *Chem. Biol.* **2015**, *22*, 619–628.

[40] Scalvini, L., Vacondio, F.; Bassi, M.; Pala, D.; Lodola, A.; Rivara, S.; Jung, K.M.; Piomelli, D.; Mor, M. Free-energy studies reveal a possible mechanism for oxidation-dependent inhibition of MGL. *Sci. Rep.* **2016**, *6*, 31046.

[41] King, A. R.; Lodola, A.; Carmi, C.; Fu, J.; Mor, M.; Piomelli, D. A critical cysteine residue in monoacylglycerol lipase is targeted by a new class of isothiazolinone-based enzyme inhibitors. *Br. J. Pharmacol.* **2009**, *157*, 974–983.

[42] Matuszak, N.; Es Saadi, B.; Labar, G.; Marchand-Brynaert, J.; Lambert, D. M. Benzisothiazolinone as a useful template for the design of new monoacylglycerol lipase inhibitors: investigation of the target residues and comparison with octhilinone. *Bioorg. Med. Chem. Lett.* **2011**, *21*, 7321–7324.

[43] McClelland, E.W.; Gait, A. J. Derivatives of 2-keto-1:2dihydrobenzisothiazole. *J. Chem. Soc.* **1926**, 921–925.

[44] Yevich, J. P.; New, J. S.; Smith, D. W.; Lobeck, W. G.; Catt, J. D.; Minielli, J. L.; Eison, M. S.; Taylor, D. P.; Riblet, L. A.; Temple, D. L. Jr. Synthesis and biological evaluation of 1-(1,2-benzisothiazol-3-yl)- and (1,2-benzisoxazol-3-yl)piperazine derivatives as potential antipsychotic agents. *J. Med. Chem.* **1986**, *29*, 359–369.

[45] Lewis, S. N.; Miller, G. A.; Hausman, M.; Szamborski, E. C. Isothiazoles I: 4-isothiazolin-3-ones. A general synthesis from 3,3′-dithiodipropionamides. *J. Heterocycl. Chem.* **1971**, *8*, 571–580.

[46] Gilday, J. P.; Lenden, P.; Moseley, J. D.; Cox, B. G. The Newman−Kwart rearrangement: a microwave kinetic study. *J. Org. Chem.* **2008**, *73*, 3130–3134.

[47] Wright, S. W.; Petraitis, J. J.; Freimark, B.; Giannaras, J. V; Pratta, M. A.; Sherk, S. R.; Williams, J. M.; Magolda, R. L.; Arner, E. C. 2,5-Diarylisothiazolone: novel inhibitors of cytokine-induced cartilage destruction. *Bioorg. Med. Chem.* **1996**, *4*, 851–858.

[48] Morreal, C. E.; Sinha, D. K.; Schneider, S. L.; Bronstein, R. E.; Dawidzik, J. Antiestrogenic Properties of Substituted Benz[a]anthracene-3,9-Diols. *J. Med. Chem.* **1982**, *25*, 323–326.

[49] Zani, F.; Vicini, P.; Incerti, M. Synthesis and antimicrobial properties of 2-(benzylidene-amino)-benzo[d] isothiazol-3-ones. *Eur. J. Med. Chem.* **2004**, *39*, 135–140.

[50] Nagayama, T.; Sinor, A. D.; Simon, R.P.; Chen, J.; Graham, S. H.; Jin, K.; Greenberg, D. A. Cannabinoids and neuroprotection in global and focal cerebral ischemia and in neuronal cultures. *J. Neurosci*. **1999**, *19*, 2987–2995.

[51] Panikashvili, D.; Simeonidou, C.; Ben-Shabat, S.; Hanus, L.; Breuer, A.; Mechoulam, R.; Shohami, E. An endogenous cannabinoid (2-AG) is neuroprotective after brain injury. *Nature* **2001**, *413*, 527–531.

[52] Hinman, A.; Chuang, H. H.; Bautista, D. M.; Julius, D. TRP channel activation by reversible covalent modification. *Proc. Natl. Acad. Sci. U S A* **2006**, *103*, 19564–19568.

[53] Macpherson, L. J.; Dubin, A. E.; Evans, M. J.; Marr, F.; Schultz, P. G.; Cravatt, B. F.; Patapoutian, A. Noxious compounds activate TRPA1 ion channels through covalent modification of cysteines. *Nature* **2007**, *445*, 541–545.

[54] Caterina, M. J.; Schumacher, M. A.; Tominaga, M.; Rosen, T. A.; Levine, J. D.; Julius, D. The capsaicin receptor: a heat-activated ion channel in the pain pathway. *Nature* **1997**, *389*, 816–824.

[55] Castillo, P.E.; Younts, T. J.; Chávez, A. E., Hashimotodani, Y. Endocannabinoid signaling and synaptic function. *Neuron* **2012**, *76*, 70–81.

[56] Katona, I.; Freund, T. F. Endocannabinoid signaling as a synaptic circuit breaker in neurological disease. *Nat. Med*. **2008**, *14*, 923–930.

[57] Cao J. K.; Kaplan, J.; Stella, N. ABHD6: its place in endocannabinoid signaling and beyond. *Trends Pharmacol. Sci*. **2019**, *40*, 267−277.

[58] Piomelli, D. The molecular logic of endocannabinoid signaling. *Nat. Rev. Neurosci*. **2003**, *4*, 873−884.

[59] Wu, L.; Lu, M.; Yan, Z.; Tang, X.; Sun, B.; Liu, W.; Zhou, H.; Yang, C. 1,2-Benzisothiazol-3-one derivatives as a novel class of small-molecule caspase-3 inhibitors. *Bioorg. Med. Chem*. **2014**, *22*, 2416–2426.

[60] Jorgensen, W. L.; Trofimov, A.; Du, X.; Hare, A. A.; Leng, L.; Bucala, R. Benzisothiazolones as modulators of macrophage migration inhibitory factor. *Bioorg. Med. Chem. Lett*. **2011**, *21*, 4545–4549.

[61] Price, K. E.; Armstrong, C. M.; Imlay, L. S.; Hodge, D. M.; Pidathala, C; Roberts, N. J.; Park, J.; Mikati, M.; Sharma, R.; Lawrenson, A. S.; Tolia, N. H.; Berry, N. G.; O'Neill, P. M.; John, A. R. Molecular mechanism of action of antimalarial benzoisothiazolones: species-selective inhibitors of the plasmodium spp. MEP pathway enzyme, IspD. *Sci. Rep*. **2016**, *18*, 6:36777.

[62] Liu, D.; Tian, Z.; Yan, Z.; Wu, L.; Ma, Y.; Wang, Q.; Liu, W.; Zhou, H.; Yang, C. Design, synthesis and evaluation of 1,2-benzisothiazol-3-one derivatives as potent caspase-3 inhibitors. *Bioorg. Med. Chem.* **2013**, *21*, 2960–2967.

[63] Kim, W.; Dannaldson, J.; Gates, K. S. Reactions of 3H-1,2-benzodithiol-3-one 1-oxide with amines and anilines. *Tetrahedron Lett.* **1996**, *37*, 5337–5340.

[64] Grivas, J. C. Novel general synthesis of 2-substituted 1,2-benzisothiazolin-3-ones. Cyclization of N-substituted 2-methoxycarbonylbenzenesulfenamides. *J. Org. Chem.* **1975**, *40*, 2029–2032.

[65] Hamieh, S.; Ludlow, R. F.; Perraud, O.; West, K. R.; Mattia, E.; Otto, S. A synthetic receptor for nicotine from a dynamic combinatorial library. *Org. Lett.* **2012**, *14*, 5404–5407.

[66] Sugiyama, H.; Yoshida, M.; Mori, K.; Kawamoto, T.; Sogabe, S.; Takagi, T.; Oki, H.; Tanaka, T.; Kimura, H.; Ikeura, Y. Synthesis and structure activity relationship studies of benzothieno[3,2-b]furan derivatives as a novel class of IKK beta inhibitors. Chem. Pharm. Bull. 2007, 55, 613–624.

[67] Liepa, A. J.; Nguyen, O.; Saubern, S. Synthesis of some 4-oxothiochromenes and related compounds. *Aust. J. Chem.* **2005**, *58*, 864–869.

[68] Archer, S.; Zayed, A. H.; Rej, R.; Rugino, T. A. Analogs of hycanthone and lucanthone as antitumor agents. *J. Med. Chem.* **1983**, *26*, 1240–1246.

[69] Douglass, I. B.; Farah, B. S. The anhydrous chlorination of some mercapto acids and analogous disulfides1,2,3. *J. Org. Chem.* **1961**, *26*, 351–354.

[70] Incerti, M.; Acquotti, D.; Vicini, P. Complete ^{1}H and ^{1}3C NMR spectral assignment of benzo[*d*]Isothiazole derivatives and of an isoindole isoster. *Magn. Reson. Chem.* **2008**, *46*, 1175–1179.

[71] Jung K. M.; Piomelli D. Assay of monoacylglycerol lipase activity. *Methods Mol. Biol*. **2016**, *1412*, 157–168.

[72] Copeland R. A. Evaluation of enzyme inhibitors in drug discovery. A guide for medicinal chemists and pharmacologists. *Methods Biochem. Anal*. **2005**, *46*, 1–265.

[73] Jung, K. M.; Astarita, G.; Zhu, C.; Wallace, M.; Mackie, K.; Piomelli, D. A key role for diacylglycerol lipase-alpha in metabotropic glutamate receptor-dependent endocannabinoid mobilization. *Mol. Pharmacol*. **2007**, *72*, 612–621.

[74] Spadoni, G.; Bedini, A.; Furiassi, L.; Mari, M.; Mor, M.; Scalvini, L.; Lodola, A.; Ghidini, A.; Lucini, V.; Dugnani, S.; Scaglione, F.; Piomelli, D.; Jung, K. M.; Supuran, C. T.; Lucarini, L.; Durante, M.; Sgambellone, S.; Masini, E.; Rivara, S. Identification of bivalent ligands with melatonin receptor agonist and fatty acid amide hydrolase (FAAH) inhibitory activity that exhibit ocular hypotensive effect in the rabbit. *J. Med. Chem*. **2018**, *61*, 7902–7916.

[75] Navia-Paldanius D.; Savinainen J. R.; Laitinen J. T. Biochemical and pharmacological characterization of human α/β-hydrolase domain containing 6 (ABHD6) and 12 (ABHD12). *J. Lipid Res.* **2012**, *53*, 2413–2424.

[76] https://euroscreenfast.com/

[77] Maestro, version 9.2; Schrödinger, LLC: New York, 2011.

[78] LigPrep, version 2.5; Schrödinger, LLC: New York, 2011.

[79] a) Schrödinger Suite 2011 Protein Preparation Wizard; Schrödinger, LLC: New York, 2011; (b) Epik version 2.2; Schrödinger, LLC, New York, NY, 2011; (c) Impact, version 5.7; Schrödinger, LLC: New York, 2011; (d) Prime, version 3.0; Schrödinger, LLC: New York, 2011.

[80] Prime, version 3.0; Schrödinger, LLC: New York, 2011.

[81] Jacobson, M. P.; Pincus, D. L.; Rapp, C. S.; Day, T. J. F.; Honig, B.; Shaw, D. E.; Friesner, R. A. A hierarchical approach to all-atom protein loop prediction. *Proteins* **2004**, *55*, 351−367.

[82] Jacobson, M. P.; Friesner, R. A.; Xiang, Z.; Honig, B. On the role of crystal packing forces in determining protein sidechain conformations. *J. Mol. Biol*. **2002**, *320*, 597−608.

[83] Glide, version 6.1; Schrödinger, LLC: New York, 2011.

[84] Friesner, R. A.; Banks, J. L.; Murphy, R. B.; Halgren, T. A.; Klicic, J. J.; Mainz, D. T.; Repasky, M. P.; Knoll, E. H.; Shelley, M.; Perry, J. K.; Shaw, D. E.; Francis, P.; Shenkin, P. S. Glide: a new approach for rapid, accurate docking and scoring. 1. Method and assessment of docking accuracy. *J. Med. Chem*. **2004**, *47*, 1739−1749.

[85] Labar, G.; Bauvois, C.; Borel, F.; Ferrer, J. L.; Wouters, J.; Lambert, D. M. Crystal structure of the human monoacylglycerol lipase, a key actor in endocannabinoid signaling. *ChemBioChem.* **2010**, *11*, 218–227.

[86] Jorgensen, W. L.; Maxwell, D. S.; Tirado-Rives, J. Development and testing of the OPLS all-atom force field on conformational energetics and properties of organic liquids. *J. Am. Chem. Soc*. **1996**, *118*, 11225−11236.

[87] MacroModel, version 9.9; Schrödinger, LLC: New York, 2011.

[88] Lomize M. A., Pogozheva I. D., Joo H., Mosberg H. I., Lomize A. L. OPM database and PPM web server: resources for positioning of proteins in membranes. *Nucleic Acids Res*. **2012**, *40,* (Database issue), D370−D376.

[89] Desmond Molecular Dynamics System D. E. Shaw Research, New York, NY, USA, 2013.

[90] Darden, T.; York, D.; Pedersen, L. Particle mesh Ewald: An N·log(N) method for Ewald sums in large systems. *J. Chem. Phys*. **1993**, *98*, 10089−10092.

[91] Nazari, Z. E.; van de Weert, M., Bou-Assaf, G.; Houde, D.; Weiskopf, A.; Rand K. D. Rapid conformational analysis of protein drugs in formulation by hydrogen/deuterium exchange mass spectrometry. *J. Pharm. Sci*. **2016**, *105*, 3269−3277.

[92] Rist, W.; Mayer, M. P.; Andersen, J. S.; Roepstorff, P.; Jørgensen, T. J. Rapid desalting of protein samples for on-line microflow electrospray ionization mass spectrometry. *Anal. Biochem*. **2005**, *342*, 160−162.

[93] Rand, K. D.; Zehl, M.; Jensen, O. N.; Jørgensen, T. J. Protein hydrogen exchange measured at single-residue resolution by electron transfer dissociation mass spectrometry. *Anal. Chem*. **2009**, *15*, 5577−5584.

[94] Protein Lynx Global Server, version 3.0; Waters, Corp: Milford, 2009.

Table of Contents Graphic